Journal for ImmunoTherapy of Cancer

TCR-engineered adoptive cell therapy effectively treats intracranial murine glioblastoma

Maximilian O Schaettler,[1] Rupen Desai ,[1] Anthony Z Wang,[1] Alexandra J Livingstone,[2] Dale K Kobayashi,[1] Andrew T Coxon,[1] Jay A Bowman-Kirigin,[3] Connor J Liu,[4] Mao Li,[5] Diane E Bender,[6] Michael J White,[7] David M Kranz,[8] Tanner M Johanns,[2] Gavin P Dunn [5]

To cite: Schaettler MO, Desai R, Wang AZ, *et al*. TCR-engineered adoptive cell therapy effectively treats intracranial murine glioblastoma. *Journal for ImmunoTherapy of Cancer* 2023;**11**:e006121. doi:10.1136/jitc-2022-006121

► Additional supplemental material is published online only. To view, please visit the journal online (http://dx.doi.org/10.1136/jitc-2022-006121).

Accepted 13 January 2023

For numbered affiliations see end of article.

Correspondence to
Dr Gavin P Dunn;
gpdunn@mgh.harvard.edu

ABSTRACT

Background Adoptive cellular therapies with chimeric antigen receptor T cells have revolutionized the treatment of some malignancies but have shown limited efficacy in solid tumors such as glioblastoma and face a scarcity of safe therapeutic targets. As an alternative, T cell receptor (TCR)–engineered cellular therapy against tumor-specific neoantigens has generated significant excitement, but there exist no preclinical systems to rigorously model this approach in glioblastoma.

Methods We employed single-cell PCR to isolate a TCR specific for the $Imp3_{D81N}$ neoantigen (mImp3) previously identified within the murine glioblastoma model GL261. This TCR was used to generate the Mutant Imp3-Specific TCR TransgenIC (MISTIC) mouse in which all CD8 T cells are specific for mImp3. The therapeutic efficacy of neoantigen-specific T cells was assessed through a model of cellular therapy consisting of the transfer of activated MISTIC T cells and interleukin 2 into lymphodepleted tumor-bearing mice. We employed flow cytometry, single-cell RNA sequencing, and whole-exome and RNA sequencing to examine the factors underlying treatment response.

Results We isolated and characterized the 3×1.1C TCR that displayed a high affinity for mImp3 but no wild-type cross-reactivity. To provide a source of mImp3-specific T cells, we generated the MISTIC mouse. In a model of adoptive cellular therapy, the infusion of activated MISTIC T cells resulted in rapid intratumoral infiltration and profound antitumor effects with long-term cures in a majority of GL261-bearing mice. The subset of mice that did not respond to the adoptive cell therapy showed evidence of retained neoantigen expression but intratumoral MISTIC T cell dysfunction. The efficacy of MISTIC T cell therapy was lost in mice bearing a tumor with heterogeneous mImp3 expression, showcasing the barriers to targeted therapy in polyclonal human tumors.

Conclusions We generated and characterized the first TCR transgenic against an endogenous neoantigen within a preclinical glioma model and demonstrated the therapeutic potential of adoptively transferred neoantigen-specific T cells. The MISTIC mouse provides a powerful novel platform for basic and translational studies of antitumor T-cell responses in glioblastoma.

WHAT IS ALREADY KNOWN ON THIS TOPIC

⇒ The targeting of tumor-specific neoantigens through T cell adoptive transfer represents an exciting avenue for further study owing to the exquisite tumor specificity of neoantigens. However, there exist very few platforms for adequate preclinical investigations of these approaches and none within glioblastoma.

WHAT THIS STUDY ADDS

⇒ In this work, we generated a novel T cell receptor transgenic against a tumor neoantigen within the murine glioma model GL261 and established the therapeutic potential of neoantigen-specific cellular therapy.

HOW THIS STUDY MIGHT AFFECT RESEARCH, PRACTICE OR POLICY

⇒ Our results suggest that neoantigen-directed cellular therapy can be effective in the treatment of murine glioblastoma but will require further investigation to overcome immune escape through T-cell dysfunction and tumor heterogeneity.

INTRODUCTION

Glioblastoma (GBM) is the most common and lethal primary tumor of the central nervous system in adults with approximately 12 000 new cases per year.[1] Significant advances in our understanding of the molecular and genetic features of GBM have not led to effective new therapies with a conventional standard-of-care treatment for primary GBM still consisting of surgery followed by concurrent chemoradiation.[2–4] Despite this multimodality treatment, patients have a poor prognosis with a median progression-free survival of 6.9 months and overall survival between 14 and 20 months.[2 5] Thus, there exists a clear need for the development of novel therapies for patients with this diagnosis.

The striking successes of immunotherapy in other cancers have stimulated a search for immune-based therapies in GBM as

well. Specifically, there is significant interest in adoptive T cell therapies for tumors such as GBM which lack significant intratumoral T cell infiltration at baseline. These tumors are therefore considered "cold" or "non-inflamed." The antigenic targets for adoptive human leukocyte antigen (HLA)-restricted T cell therapies can be broadly grouped into either non-mutated shared antigens or neoantigens produced as a result of somatic mutations in cancer development. Therapies leveraging T cell receptor (TCR)–engineered T cells against shared antigens also expressed on normal tissues have shown strong preclinical and early-phase clinical results but also generated severe toxicities.[6–9] As a result, neoantigens represent ideal therapeutic targets due to their (1) tumor-specific expression and (2) the lack of pre-existing immune tolerance. Preclinical mouse studies have shown that the recognition of neoantigens forms the basis for both immunoediting and checkpoint blockade–mediated tumor rejection.[10 11] Furthermore, the adoptive transfer of expanded tumor-infiltrating lymphocyte (TIL) cultures containing neoantigen-specific T cells has generated responses across a diverse range of cancer types.[12–14] Within GBM, adoptive T cell therapy has been limited to trials of chimeric antigen receptor (CAR) T cells generated against targets including the epidermal growth factor receptor variant III (EGFRvIII) variant, interleukin-13 receptor subunit alpha 2 (IL13Rα2) cancer/testis antigen, receptor tyrosine-protein kinase erbB-2 (Her2), and recently disialoganglioside (GD2) in pediatric brain tumors.[15–18] Together, these approaches have shown modest responses but ultimate treatment failure owing to factors such as antigen downregulation and T cell exhaustion.[15 16] However, because the potential targets for CAR T therapy are likely limited and carry possible safety issues, there is a compelling rationale to identify HLA-restricted targets to enable the development of complementary cell therapy programs.[19–21]

Despite significant interest in adoptive T cell therapy for solid tumors and the potential benefits of targeting tumor-specific neoantigens, few preclinical systems exist to accurately model this therapy. This shortcoming is due in large part to both the limited number of endogenous tumor neoantigens that have been identified in murine models and the even smaller number of known TCRs that exist to target them. Indeed, most preclinical systems for studying adoptive T cell immunotherapy target significantly overexpressed and highly immunogenic foreign proteins ectopically introduced into the tumors or shared antigens also expressed by normal tissues.[22 23] However, neither overexpressed foreign proteins nor shared antigens accurately recapitulate the tumor-specific expression profile and degree of immunogenicity of an endogenous tumor neoantigen. Thus, there exists a need for a platform to investigate neoantigen-directed cellular therapy and the role of neoantigen-specific T cells in GBM.

To that end, we have generated and characterized a TCR transgenic mouse against a tumor neoantigen within the murine GBM model GL261. Previous work from our laboratory identified the $Imp3_{D81N}$ point mutation (mImp3) as an H2-D^b-restricted class I neoantigen recognized by intracranial TIL and T cells within tumor-draining lymph nodes of GL261-bearing mice.[24] Herein, we cloned a highly reactive and specific mImp3-specific TCR to generate the Mutant Imp3-Specific TCR TransgenIC (MISTIC) mouse, a TCR transgenic for use in adoptive transfer studies. Treatment of mice bearing intracranial GL261 with adoptive cell therapy of MISTIC T cells resulted in significant intratumoral T cell infiltration and a profound increase in survival with long-term cures in a subset of mice. To our knowledge, this is the first TCR transgenic generated against a tumor-specific neoantigen in a mouse GBM model. This system displays the potential for neoantigen-targeted cellular therapy in the treatment of GBM and serves as a platform for both translational and basic investigation on the role of neoantigen-specific T cells in GBM.

RESULTS

Identification and validation of neoantigen-specific TCR

Having previously identified the $Imp3_{D81N}$ mutation (mImp3) as a class I neoantigen within the C57BL/6-derived murine glioma model GL261, we first sought to isolate a mImp3-specific TCR against this neoantigen.[24] To generate this TCR pool, three separate populations of mImp3-specific T cells were employed. Splenocytes were isolated from C57BL/6 wild-type mice that had (1) rejected GL261 tumor cells once following anti-programmed death-ligand 1 αPD-L1 therapy (1×), (2) rejected GL261 tumor cells once following aPD-L1 therapy and an additional two times following rechallenge (3×), or (3) had been vaccinated in a prime-boost manner with mImp3 synthetic long peptide and Poly(I:C) adjuvant (Vax). Each of these populations was stimulated separately in vitro with low-dose mImp3 peptide and interleukin 2 (IL-2) for a period of 6–8 weeks prior to tetramer sorting of single mImp3-specific CD8 T cells into PCR plates (figure 1A).

To isolate mImp3-specific TCRs, we adapted a previously published single-cell PCR protocol.[25] Briefly, a two-step nested PCR reaction was performed in which the first reverse-transcription-PCR (RT-PCR) reaction included a pool of 41 Vα and 39 Vβ primers specific to the leader sequences of all possible TCR-α or TCR-β chains; each primer included a common adapter sequence located 5′ to the leader sequences. The second step of the PCR amplification then generated the full TCR chain using 3′ primers specific for the constant regions and 5′ primers for the flanking adapter sequence (figure 1A). The second-step PCR products were gel-purified and then underwent Sanger sequencing for TCR sequence identification. In total, we obtained TCR-α/β pairs from 42 tetramer-sorted single cells across the three distinct populations (1×, 3×, Vax). All three groups showed a significant degree of clonal expansion among mImp3-specific CD8 T cells, with the dominant clone comprising 67%, 23%,

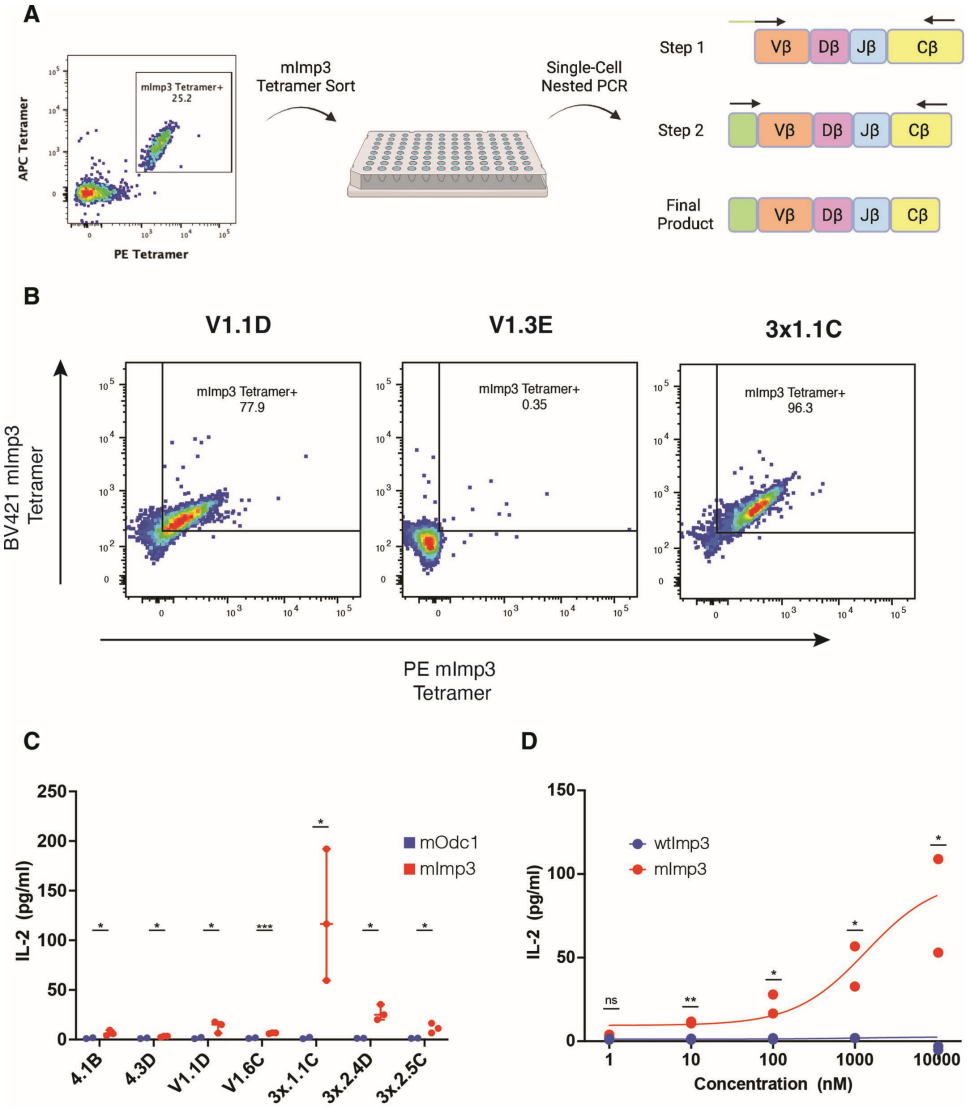

Figure 1 Identification and validation of a mutant Imp3-specific T cell receptor (TCR). (A) Overall schema for TCR identification consisting of tetramer sorting of mutant Imp3-specific T cells followed by single-cell PCR. (B) Representative flow cytometry plots demonstrating tetramer binding of candidate TCRs following cloning into $58^{-/-}$ hybridoma cells. Samples gated on TCR-expressing $58^{-/-}$ cells. (C) Interleukin 2 (IL-2) secretion from $58^{-/-}$ hybridoma cells transduced with candidate TCRs when stimulated with either mutant Imp3 or an irrelevant peptide (mOdc1). Results from three independent experiments for mImp3 ($Imp3_{D81N}$ neoantigen) and mImp2 independent experiments for mOdc1 performed in duplicate. Significance by one-sided t-test. (D) IL-2 secretion from $58^{-/-}$ hybridoma cells expressing the 3×1.1C TCR stimulated with varying concentrations of either the mutant or wild-type Imp3 epitope. Results from two independent experiments performed in duplicate. Significance by one-sided t-test.

and 45% of the cells within 1×, 3×, and Vax populations, respectively (online supplemental figure 1). From these isolated TCRs, a total of nine candidates were selected for further analysis based on their identified frequencies (online supplemental figure 2).

We used two assays to characterize the nine selected TCR candidates. Full-length TCR chains were generated by combining our PCR Sanger sequencing results with IMGT constant region reference sequences (https://www.imgt.org). To generate equal stoichiometries of α- and β-chains, cassettes were assembled in which the α- and β-chains were joined by a P2A sequence. To ectopically express each TCR cassette, we employed the previously described $58^{-/-}$ hybridoma cell line that lacks an endogenous TCR but generates robust antigen-specific responses following the introduction of a specific TCR.[26 27] Each TCR was retrovirally introduced into $CD8+58^{-/-}$ cells, generating a library of TCR-expressing hybridoma cell lines. First, TCRs were screened for their ability to bind the H-$2D^b$-mImp3 tetramer we have described previously.[24] In total, seven of the nine candidates displayed variable levels of tetramer affinity, with the 3×1.1C TCR demonstrating the strongest binding (figure 1B and online supplemental figure 3). Notably, the 3×1.1C TCR was the only candidate to bind to the H-$2D^b$-mImp3 tetramer in a CD8-independent manner

(data not shown). Interestingly, despite being isolated from tetramer-sorted CD8 T cells, the V1.3E and 3×1.4A TCRs did not bind to the D^b-mImp3 tetramer.

The seven candidate TCRs with detectable levels of tetramer binding were then assessed for their ability to stimulate cytokine production in an antigen-specific manner in TCR-expressing $58^{-/-}$ cells. All candidates induced IL-2 production when cocultured with naive splenocytes loaded with the mImp3 epitope but not an irrelevant H-$2D^b$-restricted antigen (mOdc1) we have previously described.[24] However, cells transduced with the 3×1.1C TCR produced higher levels of IL-2 compared with cells transduced with other candidates (figure 1C). To further profile this TCR, we assessed its potential cross-reactivity to the wild-type Imp3 epitope. In a similar coculture experiment, $58^{-/-}$ cells transduced with the 3×1.1C TCR displayed a clear dose-dependent response to the mImp3 antigen but no wild-type reactivity across a wide range of concentrations (figure 1D). Thus, based on the strong tetramer binding, the induction of robust cytokine secretion, and highly selective discrimination between wild-type and mutant Imp3, we selected the 3×1.1C TCR for use in developing the MISTIC preclinical model.

Generation and characterization of neoantigen-specific TCR transgenic

Using the 3×1.1C α- and β-chains, we generated the MISTIC TCR transgenic mouse to enable studies of neoantigen-directed adoptive T cell therapy (see Methods section). We first characterized MISTIC T cells to determine their specificity and reactivity to mImp3. Using flow cytometry with the H-$2D^b$-mImp3 tetramer, we showed that a majority (>90%) of the T cells within the peripheral blood of MISTIC mice were CD8+ T cells (figure 2A, left) and that nearly all recognized the mImp3 neoantigen by tetramer staining (figure 2A, right). MISTIC T cells isolated from transgenic spleens displayed low levels of activation markers such as CD69 and CD44 with correspondingly high expression of CD62L, indicating that these cells were predominantly in the naive state (figure 2B and online supplemental figure 4). However, on stimulation with 1 µM mImp3 peptide and low-dose IL-2 (30 IU/mL), MISTIC T cells proliferated and adopted an activated phenotype characterized by the upregulation of CD69 and CD44 (figure 2B and online supplemental figure 4). This activation was neoantigen-specific, as proliferation was only observed when naive MISTIC T cells were stimulated with the mutant but not wild-type Imp3 peptide (figure 2C).

We next sought to assess the functional capacity of these MISTIC T cells in response to peptide-loaded and tumor targets. After differentiation with 1 µM mImp3 peptide and low-dose IL-2, the MISTIC T cells produced IFN-γ in a dose-dependent manner in response to mImp3 peptide but not to wild-type or an irrelevant D^b-restricted peptide (mOdc1) (figure 2D). Similarly, activated MISTIC T cells secreted significant levels of IFN-γ when cocultured overnight with mImp3-expressing GL261 but not an irrelevant glioma cell line (CT2A) lacking the $Imp3_{D81N}$ mutation (figure 2E). When a fragment of the mImp3 minigene cassette encoding the D81N point mutation was retrovirally introduced into CT2A, MISTIC T cell reactivity was restored, displaying the sufficiency of the $Imp3_{D81N}$ mutation in mediating MISTIC T cell cytokine production (figure 2E). Thus, activated MISTIC T cells displayed neoantigen-specific effector functions in response to peptide-loaded or antigen-expressing targets and demonstrated that MISTIC mice could be employed as a source of naive T cells specific for the mImp3 neoantigen within GL261 for adoptive cell therapy.

MISTIC T cell adoptive cell therapy

Having characterized the phenotypic and functional states of MISTIC T cells, we aimed to assess their therapeutic capacity against established GL261 tumors. To do so, we adopted an established cell therapy protocol using in vitro T cell activation and expansion prior to transfer into lymphodepleted irradiated tumor-bearing mice in combination with IL-2 treatment[28 29] (figure 3A). GL261-bearing mice receiving only irradiation and IL-2 (control) but no MISTIC T cells all succumbed to their disease with a median survival of 23 days, in line with the survival of completely untreated GL261-bearing mice[30] (figure 3B). However, when MISTIC T cells were infused in conjunction with lymphodepletion and IL-2 (MISTIC adoptive cell therapy (ACT)) on day 7 following GL261 implantation, a significant survival benefit was observed ($p<0.0001$) (figure 3B). Following MISTIC ACT, a majority of mice were asymptomatic more than 75 days after tumor implantation. Interestingly, this survival benefit observed with treatment on day 7 was lost when the MISTIC ACT was delayed until day 14 after GL261 implantation (online supplemental figure 5).

To provide additional evidence of day 7 treatment response, cohorts of control and MISTIC ACT treated tumor-bearing mice also underwent 7 weeks of serial MRI scans beginning on day 14 after GL261 implantation. Control mice consistently showed the evidence of gross disease at day 21 with subsequent tumor growth until their death (figure 3C). However, most MISTIC ACT treated mice showed no radiographic evidence of disease throughout the course of imaging, suggesting clearance of gross disease and possible cure (online supplemental figure 6).

We next sought to examine the impact of host-derived immune cells on the MISTIC ACT effect. Considerable prior work has explored the role of the conventional type 1 dendritic cell (cDC1) in mediating antitumor immunity and the generation of antitumor CD4 and CD8 T cell responses.[31–33] To assess the importance of the cDC1 subset in MISTIC ACT, we used the *IRF8+32*$^{-/-}$ mouse previously shown to be a model of selective cDC1 deficiency.[34] GL261-bearing *IRF8+32*$^{-/-}$ mice

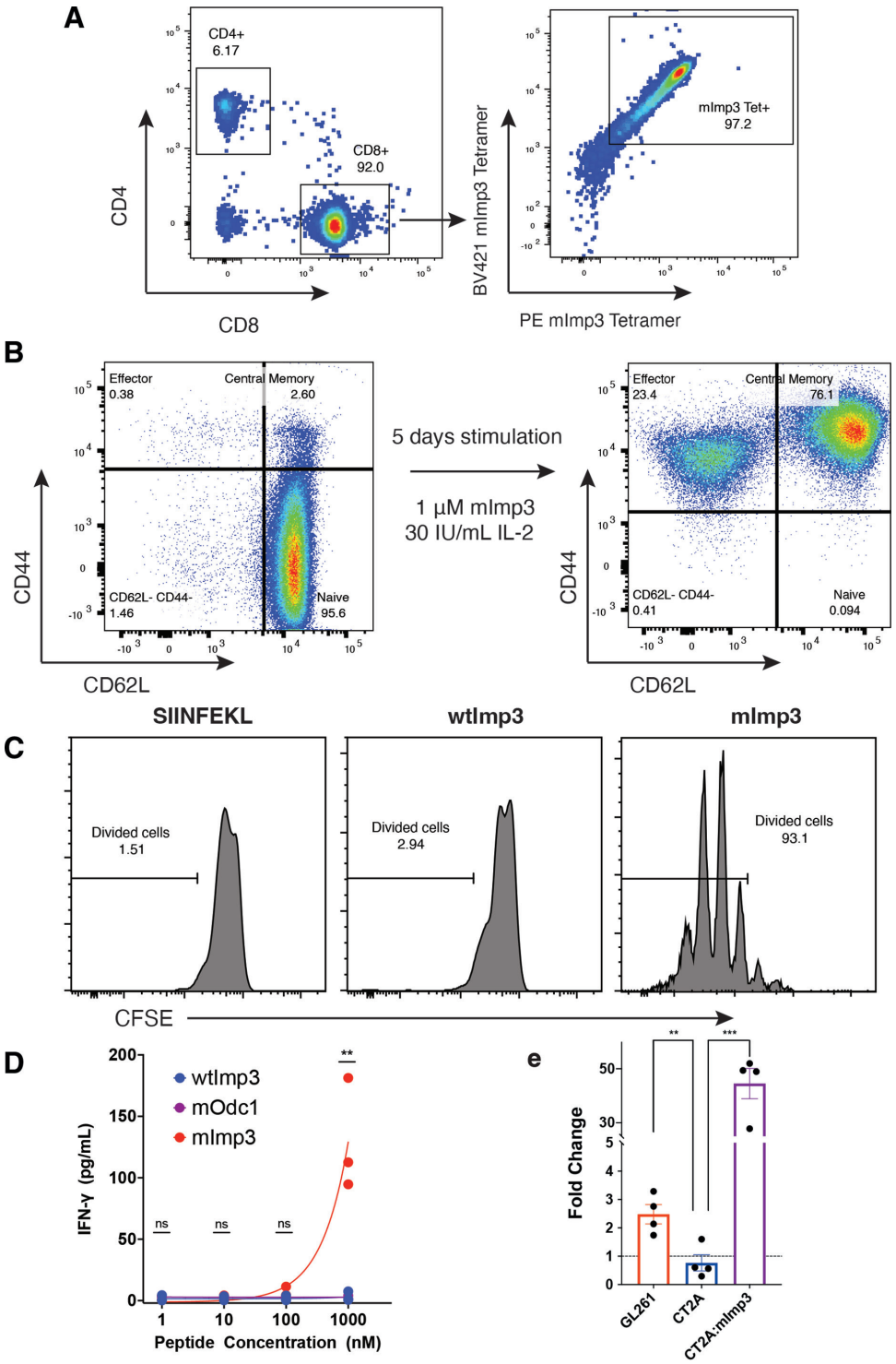

Figure 2 Generation and characterization of Mutant Imp3-Specific TCR TransgenIC (MISTIC) transgenic. (A) Representative flow cytometry from the peripheral blood of MISTIC transgenic cells. (B) Representative flow cytometry plots of naive (left) or peptide-stimulated (right) CD8 T cells from the spleens of MISTIC transgenic mice. (C) Representative results from CFSE-labeled MISTIC T cells following 48 hours of Incubation with 100 nM of indicated peptide. Representative of two independent experiments. (D) Interferon γ (IFN-γ) secretion by activated MISTIC T cells following stimulation with indicated peptide. Results from three independent experiments performed in duplicate. Significance by ANOVA (analysis of variance). (E) IFN-γ secretion (fold change above T cells alone) from MISTIC T cells following coculture with the indicated tumor lines. Results from four independent experiments. Significance by t-test. CFSE. carboxyfluorescein succinimidyl ester.

treated with MISTIC ACT on day 7 showed significantly enhanced survival ($p<0.005$) relative to *IRF8+32*$^{-/-}$ mice that did not receive MISTIC ACT but diminished survival relative to control mice treated with MISTIC ACT ($p<0.05$) (figure 3D). Finally, to assess the role of host lymphocytes in MISTIC ACT treatment, we used

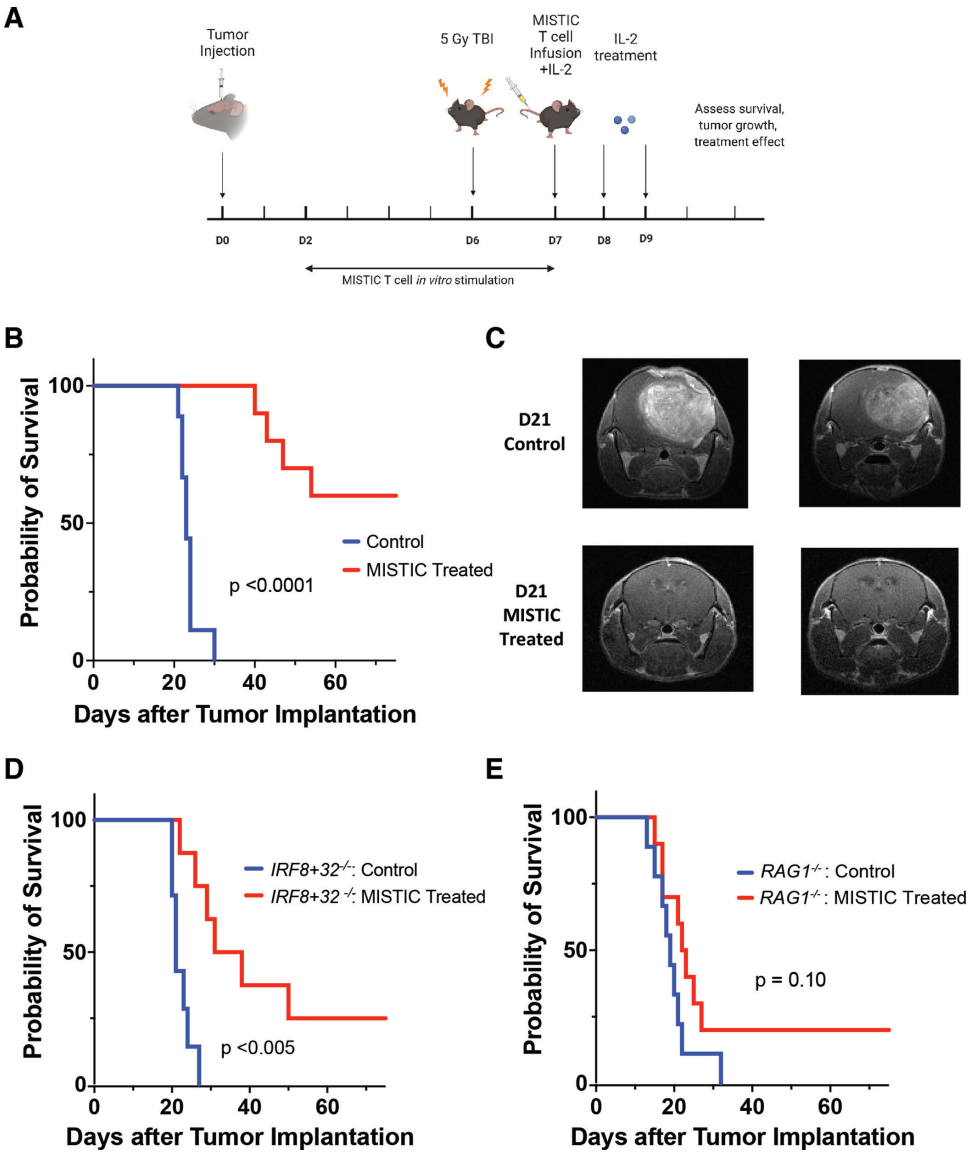

Figure 3 Efficacy of Mutant Imp3-Specific TCR TransgenIC (MISTIC) adoptive cell therapy. (A) Overall schema for day 7 MISTIC T cell treatment of tumor-bearing mice consisting of 5 days of in vitro stimulation prior to tail vein transfer, preparatory lymphodepleting irradiation, and interleukin 2 (IL-2) supplementation. (B) Survival of GL261-bearing mice treated on day 7 with either irradiation and IL-2 (control) or irradiation, IL-2, and MISTIC T cells (MISTIC treated). Significance by log-rank test with n=10 per group from two independent experiments. (C) Representative T1-weighted MRI scans of either control or day 7 MISTIC-treated mice 21 days following tumor implantation. (D) Survival of GL261-bearing *IRF8*+32$^{-/-}$ mice treated on day 7 with either irradiation and IL-2 (control) or irradiation, IL-2, and MISTIC T cells (MISTIC treated). Significance by log-rank test with n=8 per group from two independent experiments. (E) Survival of GL261-bearing RAG1$^{-/-}$ mice treated on day 7 with either IL-2 (control) or IL-2 and MISTIC T cells (MISTIC treated). Significance by log-rank test with n=10 per group from two independent experiments.

RAG1$^{-/-}$ mice lacking endogenous B or T cells. Prior studies have confirmed the ability of T cells adoptively transferred into *RAG1*$^{-/-}$ tumor-bearing hosts to infiltrate solid tumors, migrate into the central nervous system (CNS), and mediate antitumor effects.[35–38] Tumor-bearing RAG1 knockout (KO) mice treated with MISTIC ACT on day 7 showed no increase in survival on GL261 challenge (p=0.10) (figure 3E).

Having defined the therapeutic benefit of MISTIC ACT, we then aimed to characterize the distribution and differentiation state of the MISTIC T cells following transfer. Within 3 days of treatment, we found that the transferred MISTIC T cells made up a considerable fraction (>20%) of total CD8 T cells within the bone marrow, peripheral blood, spleen, and tumor with lower levels within the cervical and inguinal lymph nodes (figure 4A and online supplemental figure 7). These transferred cells were skewed to an effector (CD62L-CD44+) phenotype, most strikingly among the intratumoral T cells (online supplemental figure 8A). The infiltration of these MISTIC T cells resulted in substantial alterations to the tumor immune microenvironment

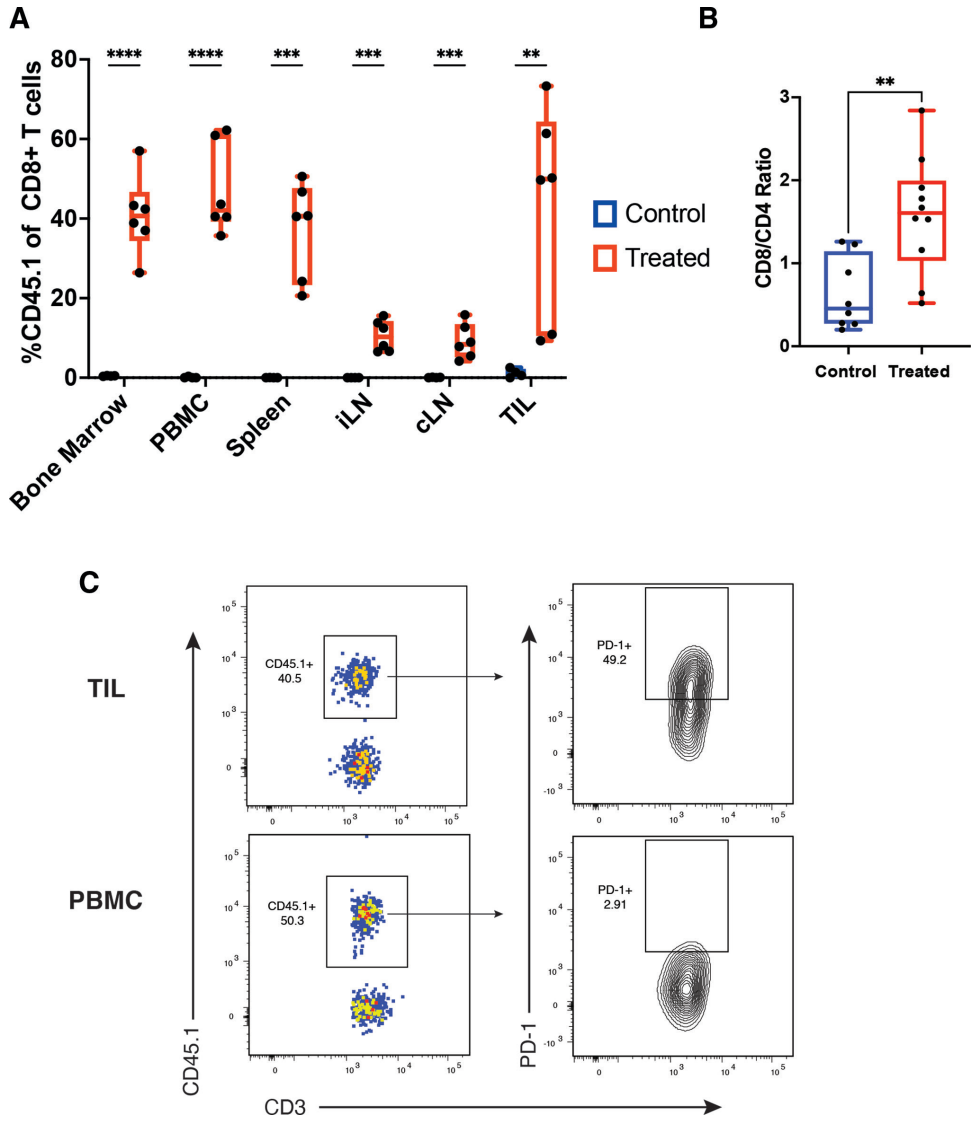

Figure 4 Characterization of Mutant Imp3-Specific TCR TransgenIC (MISTIC) adoptive cell therapy. (A) Frequency of adoptively transferred MISTIC T cells among all CD8 T cells in each indicated tissue on day 10 (3 days after adoptive transfer) following tumor implantation in either control or MISTIC-treated mice. Significance by t-test with n=6 from two independent experiments. (B) Ratio of CD8 to CD4 T cells within GL261 on day 10 (3 days after adoptive transfer) following tumor implantation in either control or MISTIC-treated mice. Significance by t-test with n=8 for control and n=10 for treated from three independent experiments. (C) Representative flow cytometry plots gated on CD8 T cells (left) or MISTIC CD8 T cells (right) in the indicated tissues on day 10 (3 days after adoptive transfer) following tumor implantation. cLN, cervical lymph node; iLN, inguinal lymph node; TIL, tumor-infiltrating lymphocyte.

within GL261 with the TIL switching from CD4 to CD8 predominant ($p<0.005$) (figure 4B). Furthermore, a significant fraction of the MISTIC T cells within both the tumor and bone marrow expressed programmed cell death protein 1 (PD-1), indicative of distinct tissue-specific expression patterns (figure 4C and online supplemental figure 8B).

Escape from MISTIC T cell therapy

Despite a significant survival benefit from MISTIC ACT, a fraction of treated mice did ultimately succumb to GL261 in a substantially delayed fashion (figure 3B). We sought to characterize these treated "escape tumors" to identify both tumor-intrinsic and tumor-extrinsic factors mediating treatment resistance. To do so, a cohort of MISTIC ACT treated escape tumors (days 40, 54, and 69 following tumor implantation) from moribund mice were analyzed via whole-exome and RNA sequencing and compared with GL261 tumors from control (irradiation and IL-2) moribund mice (days 20 and 29 following tumor implantation). All of the treated escape tumors maintained the $Imp3_{D81N}$ mutation at a comparable variant allele frequency to the untreated control tumors, indicating that genomic variant loss had not driven tumor escape in these mice (figure 5A). Furthermore, the expression of the mutant *IMP3* transcript was not different between control or treated escape tumors,

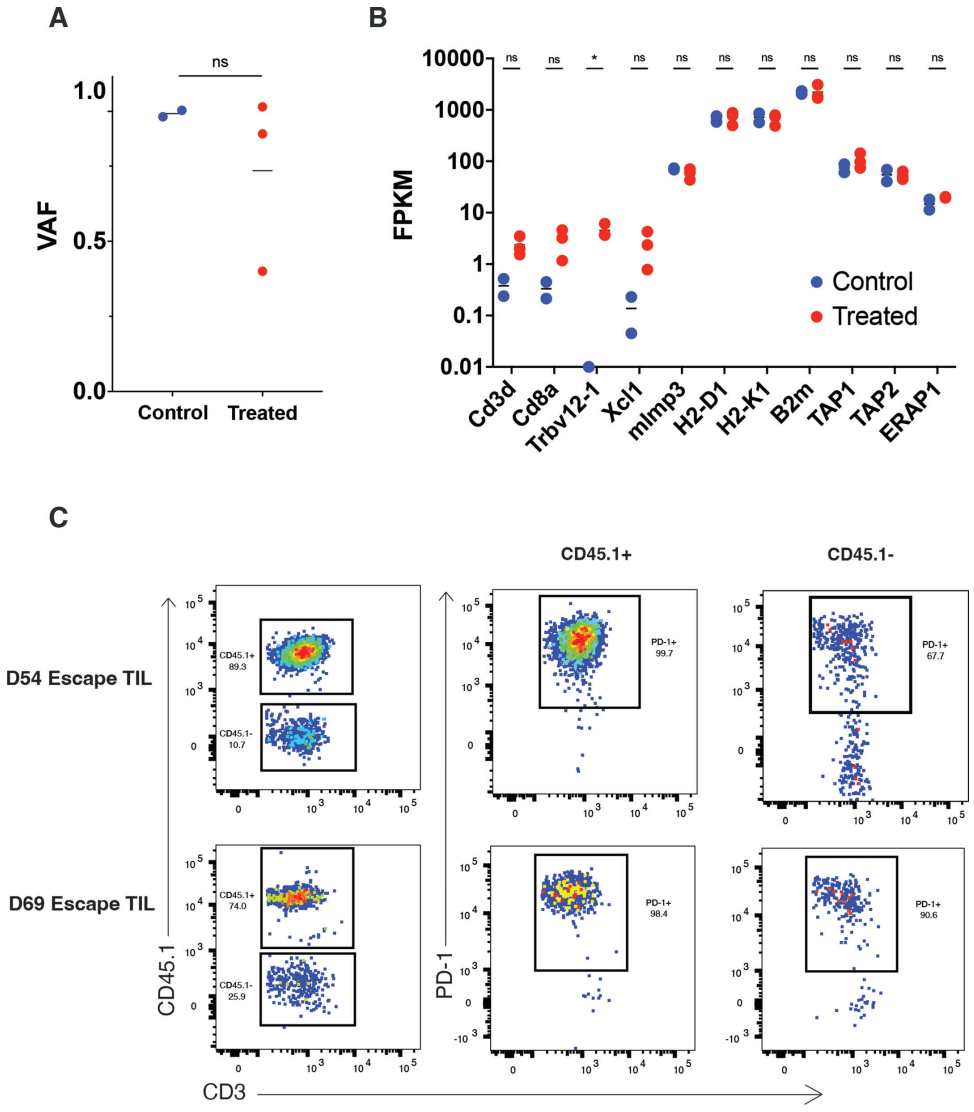

Figure 5 Profiling of Mutant Imp3-Specific TCR TransgenIC (MISTIC) ACT–treated escape tumors. (A) Variant allele frequency (VAF) of the Imp3 mutation obtained through whole-exome sequencing of GL261 tumors from control or MISTIC ACT–treated moribund mice. Significance by t-test with n=2 for control and n=3 for treated mice. (B) Gene expression for a subset of target genes from GL261 tumors isolated from control or MISTIC ACT–treated moribund mice with expression given in fragments-per-kilobase-million (FPKM). Significance by t-test with n=2 for control and n=3 for treated mice. (C) Representative flow cytometry plots gated on bulk CD8 T cells (left), MISTIC CD8 T cells (middle), or non-MISTIC CD8 T cells (right) in the indicated tumor samples on the day of harvesting from moribund mice.

suggesting that the treatment had not driven transcriptional neoantigen silencing (figure 5B). While the treated escape tumors did show the evidence of enhanced T cell infiltration with elevation of *Cd3d*, *Cd8a*, and the *Trbv12-1* gene encoding the MISTIC TCR, they retained the expression of antigen presentation machinery such as *H2-D1*, *H2-K1*, *B2m*, *TAP1*, *TAP2*, and *ERAP1* (figure 5B).

Having validated neoantigen presence at the genomic and transcriptional level, we next focused on the maintenance and functionality of MISTIC T cells in these escape tumors. Flow cytometry profiling on the immune infiltrate from these escape tumors displayed a significant MISTIC T cell infiltrate comprising a majority of all intratumoral CD8 T cells (figure 5C). Virtually all of these infiltrating MISTIC T cells expressed high levels of PD-1, potentially indicating an exhausted phenotype (figure 5C).

To more deeply characterize these intratumoral MISTIC T cells, we performed single-cell RNA sequencing (scRNA-seq) on T cells isolated from MISTIC ACT–treated escape tumors (Escape TIL), untreated control tumors (Control TIL), or MISTIC T cells expanded in vitro according to the pretreatment expansion protocol (Infusion Product). These T cells segregated into 16 distinct clusters indicating unique transcriptional states among cells isolated from three different conditions (figure 6A). The Infusion Product and Escape TIL were composed predominantly of MISTIC T cells, while the Control TIL contained a mixture of CD4+ and CD8+ T

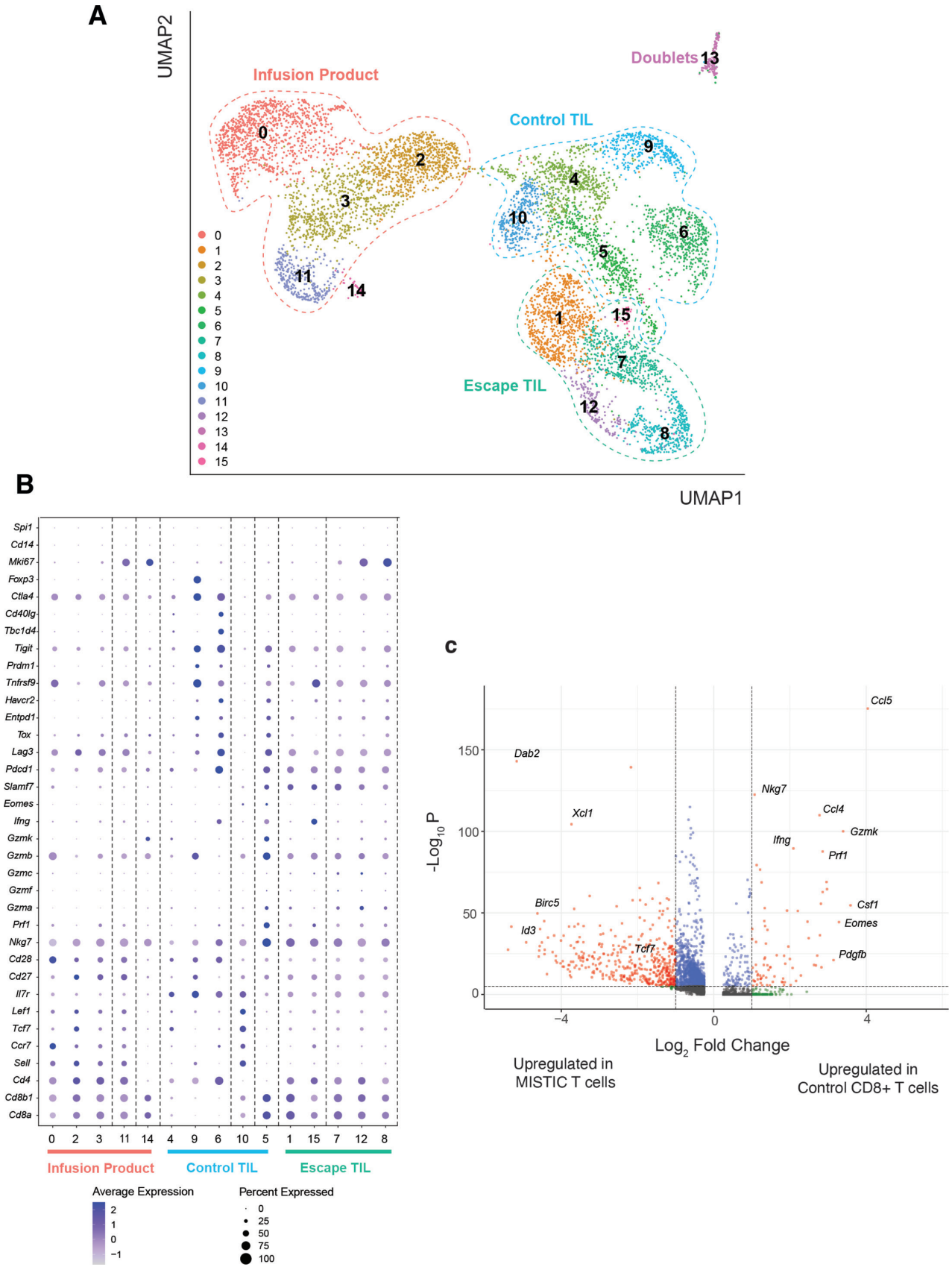

Figure 6 Single-cell profile of escape tumor-infiltrating lymphocyte (TIL). (A) Uniform manifold approximation and projection (UMAP) dimensionality reduction of the single-cell RNA sequencing (scRNA-seq) data derived from the three indicated populations. The dashed outline delineates the sample each cell derived from. (B) Dot plot of gene expression of select cell-type gene markers. (C) Volcano plot of differentially expressed genes between Mutant Imp3-Specific TCR TransgenIC (MISTIC) T cells in Escape TIL and CD8+ T cells within control TIL.

cells (online supplemental figure 9). Within the Infusion Product, both CD4+ and CD8+ T cells displayed significant skewing of TCR gene usage with a vast majority (>95%) of each population expressing the TRAV3D gene associated with the 3×1.1C TCR (online supplemental figure 10).

The CD8+ T cell clusters 7, 8, and 12 within the Escape TIL were characterized by a high proliferative rate with relatively low expression of cytotoxic markers such as *Prf1* and *Ifng* (figure 6B). In contrast, cluster 15 displayed the lowest proliferative rate among the Escape TIL but was characterized by higher expression of *Prf1*, *Ifng*, and the activation marker *Tnfrsf9* (figure 6B). We then performed differential expression analysis on the MISTIC T cells within Escape TIL compared with bulk CD8+ T cells from the Control TIL. MISTIC T cells showed the evidence of significantly diminished function with lower expression of effector molecules such as *Ifng*, *Prf1*, *Gzmb*, *Gzmk*, and *Nkg7* (figure 6C). In contrast, MISTIC T cells were enriched for markers of proliferation and memory phenotypes such as *Id3*, *Tcf7*, and *Birc5*. Of note, MISTIC T cells and control TIL CD8+ T cells displayed comparable levels of some exhaustion markers such as *Ctla4* and *Slamf7*. The two populations of T cells also displayed distinct chemokine expression patterns with Control TIL CD8+ T cells expressing significantly higher levels of *Ccl3*, *Ccl4*, *Ccl5*, and *Csf1*, while MISTIC T cells were enriched for the expression of *Xcl1* (figure 6C). Thus, the MISTIC T cells within treated escape tumors display a transcriptional program distinct from CD8+ T cells within control tumors characterized by diminished effector molecule expression and a unique chemokine expression profile.

MISTIC T cell therapy and tumor heterogeneity

Finally, given the role of tumor-cell heterogeneity and tumor antigen loss in mediating treatment resistance, we sought to assess the response to MISTIC ACT in this setting. To do so, we generated a clone of GL261, hereafter referred to as GL261:E8, in which the $Imp3_{D81N}$ point mutation was Clustered Regularly Interspaced Short Palindromic Repeats (CRISPR)-corrected to the wild-type sequence (online supplemental figure 11A). GL261 and GL261:E8 followed similar in vivo kinetics, but the wild-type correction resulted in complete loss of mImp3 tetramer-positive CD8+ T cells within intracranial TIL (figure 7A and online supplemental figure 11B).

We next assessed whether MISTIC ACT generated long-lasting immunity in mice cured of initial GL261 challenge and whether this immunity was dependent on the mImp3 neoantigen. To do so, survivor mice, defined by being symptom-free on day 60 following tumor implantation, and naive control mice were rechallenged in the contralateral hemisphere with either GL261 or GL261:E8 (figure 7B). More than 90% of survivor mice retained detectable levels of MISTIC T cells within peripheral blood prior to tumor rechallenge, and these cells were predominantly of the central memory (CD62L+CD44+) phenotype (online supplemental figure 12). These mice experienced significantly enhanced survival on rechallenge with either GL261 ($p<0.001$) or GL261:E8 ($p<0.05$) as compared with naive controls (figure 7B).

Having confirmed the efficacy of MISTIC ACT against rechallenge with an antigen-deficient subclone, we next sought to determine its effectiveness against antigen-deficient subclones in the primary setting. When mice were implanted with GL261, GL261:E8, or a 50:50 mixture of the two clones and treated on day 7 with MISTIC ACT, the response to treatment was only maintained in mice challenged with pure GL261 ($p<0.01$) (figure 7C). Targeted sequencing on the tumors recovered from moribund mice that were implanted with a 50:50 mixture displayed significant MITSIC ACT–mediated immunoediting with all treated tumors composed entirely of the mImp3-deficient GL261:E8 (figure 7D). Thus, MISTIC ACT provided limited treatment benefit in the primary setting against a heterogeneous tumor owing to the selection for antigen-deficient subclones.

DISCUSSION

Despite immense recent growth in our understanding of the molecular and genetic underpinnings of GBM, the prognosis for most patients remains poor. While cellular immunotherapies have been revolutionary in the treatment of certain cancer types, these approaches have not yet provided substantial benefit to patients with GBM. Trials of CAR T cells against EGFRvIII or IL13Ra2 have generated immense interest but few durable responses owing to antigen downregulation and T cell exhaustion.[15 16] Furthermore, CAR T cell immunotherapy necessitates the identification of suitable targets with cell surface expression profiles that provide both tumor specificity and acceptable off-target effects. TCR-engineered T cells recognizing shared tumor antigens in the context of peptide:major histocompatibility complex (MHC) restriction are an intriguing alternative strategy of engineered T cell therapy with numerous studies demonstrating robust responses across a range of solid tumors.[6 7 9 39] Broadening this approach to the targeting of tumor-specific neoantigens has become increasingly feasible with advances in immunogenomics and the tractable identification of neoantigen-specific TCRs within human TIL cultures.[13 14 40 41] Thus, we envision that some patients with GBM may be highly suitable candidates for CAR T cell approaches while others may be more appropriately treated with TCR-engineered T cell products. However, while tumor-specific neoantigens serve as attractive targets for cellular immunotherapy, no preclinical systems in which endogenous neoantigens could be targeted have been readily available to rigorously model this approach in malignant brain tumors.

To develop a model in which we could interrogate TCR-engineered therapy in GBM, we generated and characterized the MISTIC TCR transgenic mouse specific for the $H\text{-}2D^b$-restricted mImp3 neoantigen previously identified.[24] In contrast to the usage of model antigens, mImp3

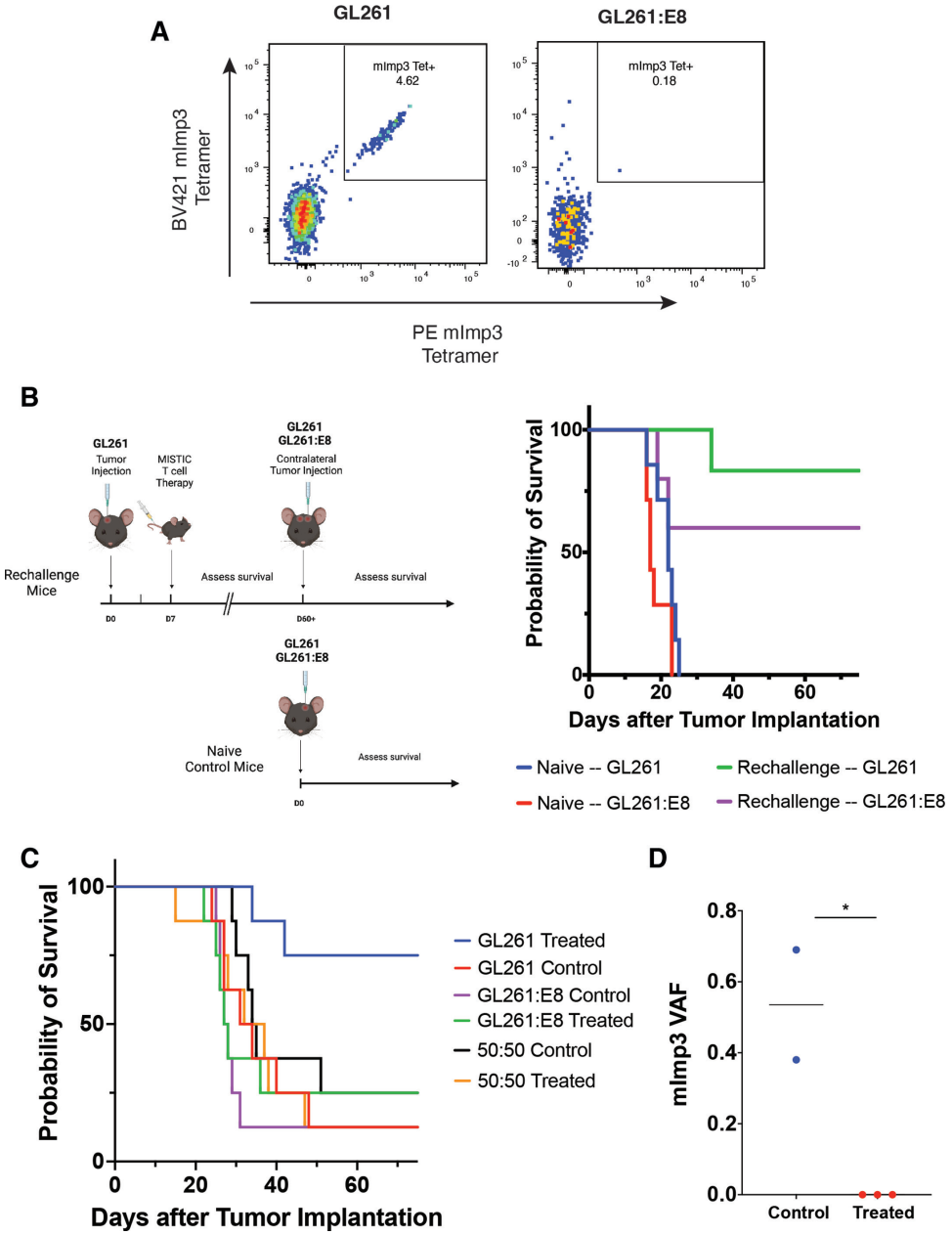

Figure 7 Impact of tumor heterogeneity on Mutant Imp3-Specific TCR TransgenIC (MISTIC) cell therapy. (A) Representative flow cytometry plots gated on intratumoral CD8 T cells within intracranial GL261 or GL261:E8 on day 16 following tumor implantation. (B) Schematic depicting tumor rechallenge experimental design (left) with associated survival curve (right). Significance by log-rank test with n=7 for naive and n=6 for rechallenge mice from two independent experiments. (C) Survival of tumor-bearing mice receiving either GL261, GL261:E8, or a 50:50 GL261-GL261:E8 mixture treated on day 7 with either irradiation and interleukin 2 (IL-2) (control) or irradiation, IL-2, and MISTIC T cells (treated). Significance by log-rank test with n=8 from two independent experiments. (D) Variant allele frequency (VAF) of the Imp3 D81N mutation in tumors isolated from control or treated moribund mice initially implanted with 50:50 GL261-GL261:E8 tumors. Significance by t-test.

more accurately recapitulates the immunogenicity and expression level of endogenous tumor targets. While the mImp3 neoantigen is endogenously recognized by intratumoral CD8+ T cells, our prior studies also displayed a protective effect from augmenting this response with therapeutic vaccination in tumor-bearing mice.[30] In the present work, we employed the MISTIC TCR transgenic system to demonstrate the efficacy of neoantigen-directed cellular therapy in a murine glioma model and to define associated changes in the tumor microenvironment. Furthermore, we employed the novel MISTIC TCR transgenic system to examine tumor-intrinsic and tumor-extrinsic factors contributing to cellular immunotherapy resistance.

Although several groups have studied CAR or TCR-engineered T cells targeting human antigens in patient xenografts, it is not possible to examine the interplay between administered therapeutic product and the immunocompetent microenvironment in settings where the host is immunocompromised.[42–45] A prior study using

TCR-based adoptive T cell therapy against a mouse neoantigen in the UV-induced 8101 cell line displayed potent antitumor effects but required the use of an immunodeficient mouse model.[46] In contrast, by studying MISTIC therapy in immunocompetent hosts, our results suggest vital roles for host cDC1s, host CD4+ and CD8+ T cells in MISTIC ACT treatment responses. Whether this requirement for endogenous immune responses is based on radiation-resistant tumor-resident T cells present at the time of treatment or the recruitment of additional specificities at later time points deserves further study. This model system also complements previous work in which tumor lines have been engineered to ectopically express model antigens or targeted tumor-associated self-antigens as therapeutic antigen targets.[22 23] However, neither overexpressed foreign proteins nor shared antigens can accurately capture the expression and immunogenicity of endogenous tumor neoantigens.

The generation of the MISTIC ACT system allows for further investigation of the factors both promoting and inhibiting response to cellular therapy. Despite the significant survival benefit provided by MISTIC ACT, a subset of mice ultimately succumb to their disease in a substantially delayed time course. Prior studies have identified numerous potential mechanisms underlying neoantigen-specific immune escape at a genomic, transcriptional, translational, and post-translational levels.[13 15 16 47 48] While our whole-exome and RNA-sequencing data support intact transcription of $Imp3_{D81N}$ and antigen presentation machinery, we cannot rule out the possibility of post-transcriptional events contributing to tumor-immune escape in our system. However, our scRNA-sequencing data suggest that intratumoral MISTIC T cells in these escape tumors displayed widely decreased effector molecule expression and a unique chemokine profile not observed in control mice. Intratumoral T cell exhaustion in GBM is often attributed to an immunosuppressive microenvironment, but the mechanisms underlying MISTIC T cell dysfunction and the extent to which it contributes to treatment failure in some mice requires additional investigation.[49–51]

We anticipate that the MISTIC ACT system will serve as a platform for further optimization of ACT for CNS cancers. Within this study, we have characterized one individual neoantigen-specific TCR, but the extent to which the ACT treatment effect could be augmented by further affinity maturation of the 3×1.1C TCR or usage of a different TCR is a focus of our future work. Additionally, the widespread usage of CRISPR technology has enabled the identification of numerous targets for potential future engineering in adoptively transferred T cells.[52–54] We anticipate that the efficacy of MISTIC ACT could be enhanced to potentially overcome tumor escape through further T cell engineering or combination therapy with checkpoint blockade.

In addition to immunosuppression and T cell dysfunction, the remarkable cellular and molecular heterogeneity within GBM has also been frequently highlighted as a cause of treatment failure.[55–59] Numerous studies have implicated that the response to clonal neoantigens is central to immunotherapy efficacy, but many therapeutic targets within GBM such as EGFRvIII display a heterogeneous expression pattern.[55 60] By generating and using the GL261:E8 line deficient in the mImp3 neoantigen, we modeled this intratumoral heterogeneity and demonstrated a clear loss of MISTIC ACT treatment effect on incorporation of antigen-deficient subclones. Intriguingly, mice cured of GL261 via MISTIC ACT showed protective immunity on rechallenge with an antigen-deficient clone, implying that some degree of epitope spreading is induced in the primary response. However, the lack of a clinical response to the GL261:E8 line in the mixing experiment suggests that the epitope spreading is insufficient to eradicate an established heterogeneous primary tumor. Taking steps to broaden epitope spreading with adjuvant therapy to improve responses to heterogeneous tumors in the primary setting will be a major focus of our future work. Overall, these results point to the clear need for further development of targeted therapies such as bispecific T cells or polyvalent vaccines that account for tumor heterogeneity.[61 62]

Beyond the efforts of this work, we envision the MISTIC transgenic system as a platform for numerous basic and translational studies on T cell and brain tumor biology. While the notion of CNS immunoprivilege has largely fallen out of favor, many nuances of the immune response to intracranial antigens remain unknown.[63 64] The MISTIC transgenic system could facilitate detailed imaging studies to address the role of the meninges as a neuroimmune interface and characterize the localization of transferred neoantigen-specific T cells. Intriguingly, a significant proportion of transferred MISTIC cells localize to the bone marrow, consistent with prior work suggesting bone marrow sequestration as a potential route of immunosuppression in GBM.[22 65] The MISTIC transgenic system will facilitate further studies within the context of an in vivo brain tumor model, identifying possible glioma-specific therapeutic targets.

Overall, this study describes the generation and characterization of the novel MISTIC TCR transgenic system and showcases both the therapeutic potential and additional avenues of therapeutic optimization of neoantigen-specific cellular therapy in GBM. We envision the MISTIC TCR transgenic will yield novel insight on both translational and basic features of the T cell response to GBM, contributing to the development of improved immunotherapies for patients with malignant brain tumors.

METHODS

Animals

Male or female mice between the ages of 6 and 16 weeks of age were used for tumor injections. To minimize the impact of animal sex on experimental results, male mice were used for all survival curves, allowing for the usage of either male or female MISTIC donor cells. Within

a given experiment, all treated mice received either male or female donor cells. A combination of male and female mice was used for adoptive transfer localization studies and validation of the GL261:E8 cell line. TCR transgenic mice were used until 1 year of age. C57BL/6 and C57BL/6:129 hybrid mice were purchased from Taconic Biosciences. CD45.1 congenic and RAG1 KO mice were purchased from Jackson Laboratory. C57BL/6 IRF8+32kb$^{-/-}$ mice were obtained from Kenneth Murphy. All mice were housed according to IACUC standards with five mice per cage. For animal experiments, cages of genetically identical age-matched mice were mixed and randomly assigned to groups that were housed adjacent to one another. They were monitored by facility staff who were blinded to their experimental condition, but no laboratory members were blinded.

Cell lines and media

GL261 was obtained from the National Cancer Institute Tumor Repository, and CT2A was obtained from Dr Peter Fecci (Duke University). All mImp3 overexpression lines were generated by cloning a 132-bp segment of the mutated *IMP3* gene into the pBabe backbone. Transduction of target cell lines was performed as described.[66] The GL261:E8 clone was generated by the Genome Engineering & iPSC Center (GEiC) at Washington University in St. Louis. Briefly, guide RNAs were designed to target near the mutation site. The parental GL261 cells were nucleofected with CRISPR constructs and single-stranded DNA donors carrying the correction. Single-cell GL261 clones were screened for the presence of the N81D correction. All tumor cell lines were maintained in D10 media consisting of Dulbecco's Modified Eagle Medium (DMEM) (Gibco) supplemented with 10% fetal bovine serum (FBS), 1% L-glutamine (Corning), 1% minimum essential media (MEM) non-essential amino acids (Corning), 1% sodium pyruvate (Lonza Bioscience), and 1% Pen/Strep (Gibco).

Fifty-eight hybridoma cells were obtained from David Kranz (University of Illinois Urbana-Champaign) and cultured in media consisting of RPMI (Gibco) supplemented with 10% FBS, 0.5% 4-(2-hydroxyethyl)-1-piperazineethanesulfonic acid (HEPES) (Corning), 1% sodium bicarbonate (Corning), 1% L-glutamine (Corning), 1% Pen/Strep (Gibco), and 50 µM β-mercaptoethanol (Sigma-Aldrich).

Primary splenocytes were cultured in R10-BME media consisting of RPMI (Gibco) supplemented with 10% FBS, 1% L-glutamine (Corning), 1% sodium pyruvate (Lonza Bioscience), 1% Pen/Strep, 0.5% sodium bicarbonate (Corning), and 50 µM β-mercaptoethanol (Sigma-Aldrich). When indicated, this media was supplemented with specific concentrations of peptide and/or cytokines.

Single-cell PCR and TCR isolation

To provide cells for TCR isolation, three separate populations of mImp3-specific T cells were generated. Splenocytes were taken from mice that had rejected GL261 once following aPD-L1 therapy (1×), once following aPD-L1 therapy and an additional two times from memory rechallenge (3×), or had been vaccinated in a prime-boost manner with 50 µg mImp3 peptide and 100 µg Poly(I:C) adjuvant (Vax). Each of these populations was stimulated with 1 nM mImp3 peptide and 50 IU/mL recombinant human interleukin-2 (rhIL-2) with a weekly replacement with fresh naive splenocytes as antigen-presenting cells. Single mImp3-specific CD8 T cells were tetramer sorted into PCR plates in a buffer of phosphate-buffered saline (PBS) with 0.1% bovine serum albumin (BSA) Fraction V (Sigma-Aldrich) and 200 U/mL RNase inhibitor (New England BioLabs) following 6–8 weeks of stimulation to enrich tetramer-positive cells.

To isolate mImp3-specific TCRs, we adopted a previously published single-cell PCR protocol.[25] In brief, a two-step nested PCR reaction was performed in which the first RT-PCR reaction included a pool of 41 Vα and 39 Vβ primers specific to the leader sequences of all possible TCR α- or β-chains. Triton X-100 detergent (Sigma-Aldrich) was added to a concentration of 0.1% for this first step to facilitate cell lysis. PCR product from this first reaction was diluted 1:100 prior to separate second-step reactions for α- or β-chains. The specific reagents used and PCR reaction conditions can be found in previously published work.[25]

The second-step PCR products were run on a gel and isolated via QIAquick Gel Extraction Kit (Qiagen) before undergoing Sanger sequencing. Full-length TCR chains were generated by combining sequencing results with IMGT (https://www.imgt.org) reference sequences for α- or β-chain constant regions. Gene blocks for each TCR were ordered (Integrated DNA Technologies) consisting of β-chain–P2A–α-chain and cloned into the pMSCV-IRES-GFP (pMIG) (AddGene) backbone through Gibson Assembly (New England BioLabs).

Hybridoma transduction and functional assays

Fifty-eight hybridoma cells were transduced with pMIG-TCR constructs through retroviruses generated as previously described.[66] Target cells were mixed with 1 mL of 58 cell media and 1 mL of 293T retroviral supernatant and spinfected at 2000 rpm for 90 min. After overnight incubation, cells were resuspended in 58 cell media and transduction efficiency was evaluated via green fluorescent protein (GFP) expression 2–3 days after transduction.

To assess functional capacity, 250 000 transduced 58 cells were cocultured with 200 000 splenocytes loaded with varying concentrations of mImp3, wild-type Imp3, or an irrelevant peptide (mOdc1). After 18 hours of incubation, plates were spun down and the supernatant was harvested and frozen prior to cytokine quantification.

Tetramer staining

Peptide-specific H-2D^{b} monomers with human β2-microglobulin were generated as previously described.[67 68] MHC class I tetramers were generated by conjugation with streptavidin-conjugated R-phycoerythrin

(PE), allophycocyanin (APC) (Invitrogen), or BV421 (BioLegend). For staining, 58 hybridoma cells or transgenic T cells were treated with dasatinib for 30 min prior to dual staining with PE- and either APC- or BV421-peptide:MHC class I tetramers for 30 min and 15 min of surface antibody staining. Fifty-eight hybridoma cells were stained with PerCP-Cy5.5-CD8, PE-Cy7-CD4, PE-Tetramer, APC-Tetramer, and Live/Dead Zombie Viability Dye. GFP expression was measured in the FITC channel, and Live/Dead Zombie Viability Dye was measured in the APC/Cy7 channel. Transgenic T cells were stained with PerCP-Cy5.5-CD45.1, FITC-CD3, PE-Cy7-CD8, PE-Tetramer, Alexa Fluor 700-CD45.2, APC-CD4, BV421-Tetramer, and Live/Dead Zombie Viability Dye (measured in APC/Cy7). All samples were stained in FACS buffer (PBS+2% FBS) with appropriate Fc block. All antibodies were purchased from BioLegend unless otherwise specified. Samples were analyzed on a BD X20 Fortessa flow cytometer.

Transgenic generation

Complete α- and β-chains from the 3×1.1C TCR were cloned into the pCD2 and p428 transgene vectors prior to pronuclear injection as previously described.[69–71] Following the digestion of pCD2 with ClaI/XbaI and p428 with NotI, purified DNA transgene fragments of the α- and β-chains were separately diluted to 2 ng/µL. Equal volumes of each chain were combined to provide the α/β-chain microinjection mixture which was coinjected into pronuclei of the single-cell d0.5 C57BL/6/129S6 F1 x C57BL/6 zygotes using standard procedures.[72] Injected zygotes were then transferred into d0.5 pseudo-pregnant female recipient mice.

To assess for transgene integration, offspring mice were screened via PCR on tail DNA using a 5′ primer specific for the given transgene plasmid and a 3′ primer specific for the CDR3 of the α- or β-chain, respectively. Mice with a positive PCR on tail DNA were then screened for TCR expression via tetramer stains on peripheral blood obtained via cheek bleed. The MISTIC Tg founder was then bred with CD45.1 C57BL/6 to produce congenically labeled MISTIC Tg mice.

MISTIC T cell stimulation and differentiation

Naive splenocytes from transgenic mice were isolated by mechanical dissociation and filtration through a 100-micron cell strainer. Mononuclear cells were isolated through Ficoll-Paque PLUS density gradient (Cytiva) centrifugation and stimulated in R10-BME media with 1 µM mImp3 peptide and 30 IU/mL rhIL-2. Cells were split 1:1 after 3 days of stimulation. After 5 days of stimulation, CD8 T cells were isolated through negative selection via EasySep Mouse CD8+ T Cell Isolation Kit (StemCell Technologies). The resulting cells were then used for select in vitro functional assays or in vivo adoptive transfer studies.

MISTIC T cell functional assays

To assess the proliferative potential of MISTIC T cells, bulk MISTIC splenocytes were carboxyfluorescein succinimidyl ester (CFSE)-labeled and cocultured for 72 hours prior to staining with PerCP-Cy5.5-CD3, PE-Cy7-CD45.2, PE-CD8, APC-CD4, BV421-CD45.1, BV605-CD62L, and Live/Dead Zombie Viability Dye (measured in APC/Cy7) before being run on a BD X20 Fortessa flow cytometer. All samples were stained in FACS buffer (PBS+2% FBS) with appropriate Fc block. All antibodies were purchased from BioLegend unless otherwise specified. CFSE fluorescence was measured in the FITC channel.

To assess the cytokine production of MISTIC T cells, they first underwent 5 days of activation as described above. After this stimulation period, all media was washed off, the cells were rested for 6 hours in low-dose IL-2, and they were cocultured overnight with peptide-loaded or tumor targets. Peptide targets were 100 000 naive splenocytes loaded with varying concentrations of the indicated peptide. Tumor targets were stimulated with 250 IU/mL IFN-γ for 1 day prior to coculture and incubated with activated MISTIC T cells at a 3:1 E:T ratio. After 18 hours of incubation, plates were spun down and supernatant was harvested and frozen prior to cytokine quantification.

Cytokine quantification

Samples were thawed on ice, centrifuged at 15 000 rcf for 5 min at 4°C to remove particulates, then 50 µL of supernatant or standard or control was added per well (in duplicate) with premixed beads and assay buffer in a 96-well plate according to manufacturer instructions (ThermoFisher High Sensitivity Procartaplex Mouse IL-2 and Interferon gamma Simplex Kits EPXS010-20601-901 and EPXS010-20606-901). The plate was incubated overnight on a shaker at 4°C, and the final detection steps and machine analyses were performed the next morning. The beads were read for mean fluorescence intensity (MFI) using a FLEXMAP3D Luminex (Luminex, Austin, Texas, USA) machine. Analysis software MilliporeSigma Belysa v.1 was used to calculate the picogram per milliliter for each analyte using a five-parameter logistical curve fit algorithm.

Flow cytometry for MISTIC Tg profiling

For profiling activated MISTIC splenocytes after 5 days of stimulation, they were stained with FITC-CD3, PE-Cy7-CD45.2, PE-CD8, PE-CF594-CD44, PE-CD8, APC-CD4, BV421-CD45.1, BV605-CD62L, and Live/Dead Zombie Viability Dye (measured in APC/Cy7). For the profiling of adoptively transferred MISTIC cells across tissues, cells were stained with PerCP-Cy5.5-CD8, FITC-CD3, PE-Cy7-CD45.2, PE-CF594-CD44, PE-PD-1, APC-CD4, BV421-CD45.1, BV605-CD62L, and Live/Dead Zombie Viability Dye (measured in APC/Cy7). All samples were stained for 30 min in FACS buffer (PBS+2% FBS) with appropriate Fc block prior to resuspension and analysis on a BD X20 Fortessa flow cytometer. All antibodies were purchased from BioLegend unless otherwise specified.

Intracranial injections

For intracranial tumor injections, cells were harvested following at least one passage and having reached 60%–90% confluency. About 50 000 tumor cells in 5 µL PBS were injected into the right hemisphere 2 mm posterior to bregma at a depth of 3.5 mm using a Stoelting stereotactic headframe. Mice were anesthetized for the procedures with ketamine/xylazine and received a long-lasting buprenorphine injection for postoperative pain. The number of mice injected in a given session was limited to 20 to limit the time each cell line was stored on ice prior to implantation. The sample size for each experiment was adjusted accordingly (usually n=5 per group) to facilitate reliable tumor implantation and growth. Following tumor injection, mice were tracked daily and euthanized when moribund as evidenced by neurological dysfunction. Mice who did not recover following tumor implantation or became sick or died during the first 2–3 days following tumor implantation were excluded from analysis due to postoperative complications. No other animals were excluded from later analyses.

Adoptive cell therapy

One day prior to receiving cell therapy, tumor-bearing mice received 5 Gy of total-body irradiation. Stimulation of naive splenocytes from transgenic mice was performed as described. After 5 days of stimulation and cell isolation, CD8 T cells were resuspended in PBS at 2.5×10^7 cells/mL and 200 µL was given intravenously via the tail vein with a 27-gauge needle. In addition, mice received daily injections of 180 000 IU of rhIL-2 intraperitoneally on the day of cell transfer and for 2 days thereafter.

MR imaging

MR imaging was performed with a 4.7-T small-animal MR scanner (Agilent/Varian, Santa Clara, California, USA) employing an actively decoupled coil pair: a 9-cm-inner-diameter volume coil (transmit) and a 1.5-cm-outer-diameter surface coil (receive). Before all imaging experiments, mice were anesthetized with isoflurane/O_2 (2% (vol/vol)) and maintained on isoflurane/O_2 (1% (vol/vol)) throughout the experiment. Mice were restrained in a laboratory-built, three-point, Teflon head holder and were placed on a water pad with circulating warm water to maintain body temperature at approximately 37±1°C. Before being placed into the magnet, each mouse was injected intraperitoneally with 0.25 mL of MultiHance (gadobenate dimeglumine; Bracco Diagnostics, Princeton, New Jersey, USA) contrast agent, diluted 2:10 in sterile saline. Postcontrast T1-weighted (T1W) images were acquired with the following parameters: time-to-repetition (TR)=650 ms, time-to-echo (TE)=11 ms, number of transient=4, field of view=15×15 mm^2, matrix size=128×128, slice thickness=0.5 mm, and 21 slices to cover the whole brain. T2-weighted images were collected with TR=1200 ms and TE=50 ms, with all other parameters the same as for the T1W images.

Tissue processing

Peripheral blood was centrifuged at 1500 rpm for 10 min and resuspended in ACK Lysis Buffer (Lonza Biosciences) for 5 min. The resultant pellet was resuspended and stained for flow cytometry.

Spleens, inguinal lymph nodes, and cervical lymph nodes were all manually dissociated using frosted microscope slides and gentle trituration. Splenocytes were filtered through a 100-micron cell strainer, and mononuclear cells were isolated using Ficoll-Paque PLUS density gradient (Cytiva) centrifugation. Lymph nodes were filtered through serial 100-micron and 70-micron cell strainers. The resultant pellets were resuspended and stained for flow cytometry or other experiments.

To extract bone marrow, the femur and tibia were dissected with scissors and forceps with surrounding tissue manually removed. The bones were kept on ice and hydrated in Hanks' Balanced Salt Solution (HBSS)+5% FBS. The ends of each bone were removed with the scissors, and a 25 G needle attached to a syringe with 10 mL of HBSS+5% FBS was used to flush the marrow out of each bone and through a 70-micron cell strainer. The resultant pellet was resuspended in ACK Lysis Buffer for 5 min prior to flow cytometry analysis.

Tumors were manually dissociated using frosted microscope slides and gentle trituration. The resulting single-cell suspension was passed through 100-micron and 70-micron cell strainers before undergoing Percoll (GE Healthcare Life Sciences) density gradient centrifugation to remove myelin contamination. Following this separation, the resulting cell pellet underwent RBC lysis with ACK Lysis Buffer (Lonza Biosciences) before being either frozen down for later analysis or stained for flow cytometry.

Tumor DNA and RNA sequencing

Total RNA and genomic DNA was extracted from frozen tumor tissue using the Qiagen AllPrep DNA/RNA Kit (catalog no 80204) according to the manufacturer's instructions (Qiagen, Valencia, California, USA). Library preparation and whole-exome sequencing was performed at a depth of 100× through Novogene on the Illumina NovaSeq 6000. Read alignment, somatic variant calling, variant annotation, and variant allele frequencies were performed through Novogene's whole-exome sequencing bioinformatics pipeline. Variant calling was performed relative to C57BL/6 tail DNA. Library preparation and RNA-sequencing was also performed through Novogene using the NovaSeq 6000 with 50M PE reads. Gene and transcript quantification was performed through Novogene's RNA-sequencing bioinformatics pipeline using the GRCm38/mm10 reference genome.

Single-cell sample and library preparation

Tumor samples were harvested as previously described. The resultant cell pellets were frozen until further analysis. On the day of sample submission, tumor and control samples were thawed and stained with FITC-CD45 and

Zombie Live/Dead Viability Dye (measured in APC/Cy7) prior to FACS sorting on live CD45+ cells. Samples were sorted into a buffer of PBS+0.04% BSA prior to sample submission for library preparation.

To generate the library for single-cell sequencing, approximately 17 500 cells were partitioned into nanoliter droplets to achieve single-cell resolution for ~10 000 individual cells per sample using the 10X Genomics Chromium Single Cell 5' v2 Library Kit and Chromium instrument. Complementary DNA (cDNA) was prepared after the gel bead-in-emulsion (GEM) generation and barcoding, followed by the GEM reverse transcription (GEM-RT) reaction and bead cleanup steps. Purified cDNA was amplified for 13 cycles before being cleaned up using SPRIselect beads. Samples were then run on an Agilent Bioanalyzer to determine the cDNA concentration. GEX and TCR libraries were prepared as recommended by the 10× Genomics Chromium Single Cell 5′ Reagent Kits User Guide (v2 Chemistry Dual Index) with appropriate modifications to the PCR cycles based on the calculated cDNA concentration. For sample preparation on the 10× Genomics platform, the Chromium Next GEM Single Cell 5′ Kit v2, 16 rxns (PN-1000263), Chromium Single Cell TCR Amplification Kits, Mouse 16 rxns (PN-1000254), Chromium Next GEM Chip K Single Cell Kit, 48 rxns (PN-1000286), and Dual Index Kit TT Set A, 96 rxns (PN-1000215) were used. The concentration of each GEX and TCR library was accurately determined through quantitative PCR using the KAPA Library Quantification Kit according to the manufacturer's protocol (KAPA Biosystems/Roche) to produce cluster counts appropriate for the Illumina NovaSeq6000 instrument. Normalized libraries were sequenced on a NovaSeq6000 S4 Flow Cell using the XP workflow and a 50×10×16×150 sequencing recipe according to manufacturer protocol. A median sequencing depth of 50 000 reads/cell was targeted for each Gene Expression Library and 5000 reads/cell for each TCR Library.

Single-cell sequencing analysis

Raw sequencing data were processed with the CellRanger pipeline (10× Genomics, default settings, version 5.0.1) mapped onto a mouse genome mm10-2020-A. All mouse samples were processed initially with the Cellbender R package and subsequently with the Seurat R package.[73 74] Cells that contained fewer than 500 features, more than 3.5% mitochondrial transcripts, and a nCount value greater than the 93rd percentile of each individual sample were removed. Samples were merged and subsequently log normalized after which variable features were selected according to default settings. Principal component analysis was then performed, and the optimal number of principal components (PCs) was determined based on results from the elbow plots, jackstraw resampling, and PC expression heatmaps (n=35). Dimensionality reduction and visualization were performed with the uniform manifold approximation and projection (UMAP) algorithm Seurat implementation, and unsupervised graph-based clustering was performed at a resolution of 1.0.[75] Cell cycle phase was assessed based on the expression of phase-specific genes following the methodology provided by Seurat.[76]

T cells were classified based on *CD3E* expression, subsetted, and all TCR segment genes were removed from the data set. Variable features were again selected according to default settings and PCA was performed after which the optimal number of principal components were selected (n=20). Dimensionality reduction and visualization were performed with UMAP and unsupervised graph-based clustering was performed at a resolution of 1.0. Differentially expressed genes of each cluster resolved by unsupervised graph-based clustering were determined using a Wilcoxon rank-sum test–based function. These genes, along with commonly defined markers, were used to identify cell identity.

Raw TCR sequencing data were processed with the CellRanger V(D)J pipeline (10× genomics, default settings, version 5.0.1) mapped onto a mouse VDJ reference GRCm38_alts_ensmbl-5.0.0. Clonotype analysis was performed using the scRepertoire R package.[77] MISTIC T cells were identified and labeled according to the expression of the 3×1.1C TCR.

Statistical analysis

Statistical significance for comparisons between groups was calculated using unpaired t-tests. Survival curve significance was assessed using log-rank tests. A p-value <0.05 was considered statistically significant, and statistical analysis was performed with GraphPad Prism 9 unless otherwise noted. The specific statistical test used for each experiment is outlined in the associated figure legend.

Author affiliations
[1]Department of Neurological Surgery, Washington University School of Medicine, St. Louis, Missouri, USA
[2]Department of Medicine, Washington University School of Medicine, St. Louis, Missouri, USA
[3]Department of Medicine, Emory University School of Medicine, Atlanta, Georgia, USA
[4]Department of Neurosurgery, Johns Hopkins University, Baltimore, Maryland, USA
[5]Department of Neurosurgery, Massachusetts General Hospital, Boston, Massachusetts, USA
[6]Bursky Center for Human Immunology & Immunotherapy Programs, Washington University School of Medicine, St. Louis, Missouri, USA
[7]Department of Pathology & Immunology, Washington University School of Medicine, St. Louis, Missouri, USA
[8]Biochemistry, University of Illinois Urbana-Champaign, Urbana, Illinois, USA

Twitter Rupen Desai @RupenDesaiMD

Acknowledgements We would like to thank the Genome Engineering and iPSC Center (GEiC) at the Washington University in St. Louis for their cell line engineering services that produced the N81D correction in the GL261 cell line. We also thank Tammi Vickery of the Immunomonitoring Lab for her assistance with nucleic acid extractions. We would also like to thank BioRender.com for a platform for the generation of figures 1A, 3A, and 7B.

Contributors MOS and GPD conceptualized the study and wrote the original manuscript. MOS and TMJ performed the in vitro experiments leading to TCR identification. MOS, RD, AL, DKK, and AC performed the tumor injections and cellular therapy infusions. MOS, RD, and AZW analyzed the data and generated the original figures. DEB performed the cytokine quantification. MJW led the generation

of the MISTIC transgenic. JAB-K, CJL, ML, DMK, and TMJ provided valuable editorial input to the final manuscript. All authors read and approved the final manuscript. GPD is responsible for the overall content as guarantor.

Funding This work was supported by the Cancer Research Institute Lloyd J Old STAR Award. MOS was supported in part by grants from the National Institutes of Health (T32GM007200-42/43/47 and T32AI007163-41A1/42).

Competing interests None declared.

Ethics approval All animal studies were approved by the Washington University Animal Studies Committee (Pprotocol #no 20180057), and all mice were housed in accordance with the Institutional Animal Care and Use Committee (IACUC; Aassurance #no A-3381—01) standards.

Provenance and peer review Not commissioned; externally peer reviewed.

Data availability statement Data are available on reasonable request. All data provided and described within the study are available on reasonable request. Inquiries may be made to gpdunn@mgh.harvard.edu.

ORCID iDs
Rupen Desai http://orcid.org/0000-0002-2052-7243
Gavin P Dunn http://orcid.org/0000-0001-9302-4834

REFERENCES

1 Ostrom QT, Gittleman H, Truitt G, *et al*. CBTRUS statistical report: primary brain and other central nervous system tumors diagnosed in the united states in 2011-2015. *Neuro Oncol* 2018;20:iv1–86.
2 Stupp R, Mason WP, van den Bent MJ, *et al*. Radiotherapy plus concomitant and adjuvant temozolomide for glioblastoma. *N Engl J Med* 2005;352:987–96.
3 Cancer Genome Atlas Research Network. Comprehensive genomic characterization defines human glioblastoma genes and core pathways. *Nature* 2008;455:1061–8.
4 Brennan CW, Verhaak RGW, McKenna A, *et al*. The somatic genomic landscape of glioblastoma. *Cell* 2013;155:462–77.
5 Weller M, Butowski N, Tran DD, *et al*. Rindopepimut with temozolomide for patients with newly diagnosed, egfrviii-expressing glioblastoma (act IV): a randomised, double-blind, international phase 3 trial. *Lancet Oncol* 2017;18:1373–85.
6 Morgan RA, Chinnasamy N, Abate-Daga D, *et al*. Cancer regression and neurological toxicity following anti-MAGE-A3 TCR gene therapy. *J Immunother* 2013;36:133–51.
7 Parkhurst MR, Yang JC, Langan RC, *et al*. T cells targeting carcinoembryonic antigen can mediate regression of metastatic colorectal cancer but induce severe transient colitis. *Mol Ther* 2011;19:620–6.
8 Johnson LA, Morgan RA, Dudley ME, *et al*. Gene therapy with human and mouse T-cell receptors mediates cancer regression and targets normal tissues expressing cognate antigen. *Blood* 2009;114:535–46.
9 Morgan RA, Dudley ME, Wunderlich JR, *et al*. Cancer regression in patients after transfer of genetically engineered lymphocytes. *Science* 2006;314:126–9.
10 Matsushita H, Vesely MD, Koboldt DC, *et al*. Cancer exome analysis reveals a T-cell-dependent mechanism of cancer immunoediting. *Nature* 2012;482:400–4.
11 Gubin MM, Zhang X, Schuster H, *et al*. Checkpoint blockade cancer immunotherapy targets tumour-specific mutant antigens. *Nature* 2014;515:577–81.
12 Zacharakis N, Chinnasamy H, Black M, *et al*. Immune recognition of somatic mutations leading to complete durable regression in metastatic breast cancer. *Nat Med* 2018;24:724–30.
13 Tran E, Robbins PF, Lu Y-C, *et al*. T-Cell transfer therapy targeting mutant KRAS in cancer. *N Engl J Med* 2016;375:2255–62.
14 Tran E, Turcotte S, Gros A, *et al*. Cancer immunotherapy based on mutation-specific CD4+ T cells in a patient with epithelial cancer. *Science* 2014;344:641–5.
15 O'Rourke DM, Nasrallah MP, Desai A, *et al*. A single dose of peripherally infused egfrviii-directed CAR T cells mediates antigen loss and induces adaptive resistance in patients with recurrent glioblastoma. *Sci Transl Med* 2017;9:eaaa0984.
16 Brown CE, Badie B, Barish ME, *et al*. Bioactivity and safety of IL13Rα2-redirected chimeric antigen receptor CD8+ T cells in patients with recurrent glioblastoma. *Clin Cancer Res* 2015;21:4062–72.
17 Ahmed N, Brawley V, Hegde M, *et al*. Her2-Specific chimeric antigen receptor-modified virus-specific T cells for progressive glioblastoma: a phase 1 dose-escalation trial. *JAMA Oncol* 2017;3:1094–101.
18 Majzner RG, Ramakrishna S, Yeom KW, *et al*. GD2-CAR T cell therapy for H3K27M-mutated diffuse midline gliomas. *Nature* 2022;603:934–41.
19 Morgan RA, Yang JC, Kitano M, *et al*. Case report of a serious adverse event following the administration of T cells transduced with a chimeric antigen receptor recognizing ErbB2. *Mol Ther* 2010;18:843–51.
20 Richman SA, Nunez-Cruz S, Moghimi B, *et al*. High-affinity GD2-specific CAR T cells induce fatal encephalitis in a preclinical neuroblastoma model. *Cancer Immunol Res* 2018;6:36–46.
21 Richman SA, Milone MC. Neurotoxicity associated with a high-affinity GD2 CAR-response. *Cancer Immunol Res* 2018;6:496–7.
22 Prins RM, Shu CJ, Radu CG, *et al*. Anti-Tumor activity and trafficking of self, tumor-specific T cells against tumors located in the brain. *Cancer Immunol Immunother* 2008;57:1279–89.
23 Nakashima H, Alayo QA, Penaloza-MacMaster P, *et al*. Modeling tumor immunity of mouse glioblastoma by exhausted $CD8^+$ T cells. *Sci Rep* 2018;8:208.
24 Johanns TM, Ward JP, Miller CA, *et al*. Endogenous neoantigen-specific CD8 T cells identified in two glioblastoma models using a cancer immunogenomics approach. *Cancer Immunol Res* 2016;4:1007–15.
25 Hamana H, Shitaoka K, Kishi H, *et al*. A novel, rapid and efficient method of cloning functional antigen-specific T-cell receptors from single human and mouse T-cells. *Biochem Biophys Res Commun* 2016;474:709–14.
26 Harris DT, Hager MV, Smith SN, *et al*. Comparison of T cell activities mediated by human tcrs and cars that use the same recognition domains. *J Immunol* 2018;200:1088–100.
27 Stone JD, Harris DT, Soto CM, *et al*. A novel T cell receptor single-chain signaling complex mediates antigen-specific T cell activity and tumor control. *Cancer Immunol Immunother* 2014;63:1163–76.
28 Klebanoff CA, Gattinoni L, Palmer DC, *et al*. Determinants of successful CD8+ T-cell adoptive immunotherapy for large established tumors in mice. *Clin Cancer Res* 2011;17:5343–52.
29 Hanada K-I, Yu Z, Chappell GR, *et al*. An effective mouse model for adoptive cancer immunotherapy targeting neoantigens. *JCI Insight* 2019;4:e124405.
30 Liu CJ, Schaettler M, Blaha DT, *et al*. Treatment of an aggressive orthotopic murine glioblastoma model with combination checkpoint blockade and a multivalent neoantigen vaccine. *Neuro-Oncology* 2020;22:1276–88.
31 Hildner K, Edelson BT, Purtha WE, *et al*. Batf3 deficiency reveals a critical role for cd8alpha+ dendritic cells in cytotoxic T cell immunity. *Science* 2008;322:1097–100.
32 Bowman-Kirigin JA, Saunders BT, Desai R, *et al*. the conventional dendritic cell 1 subset primes $CD8^+$ T cells and traffics tumor antigen to drive anti-tumor immunity in the brain . *Immunology* [Preprint] 2021.
33 Ferris ST, Durai V, Wu R, *et al*. Cdc1 prime and are licensed by CD4+ T cells to induce anti-tumour immunity. *Nature* 2020;584:624–9.
34 Durai V, Bagadia P, Granja JM, *et al*. Cryptic activation of an IRF8 enhancer governs cdc1 fate specification. *Nat Immunol* 2019;20:1161–73.
35 Arina A, Schreiber K, Binder DC, *et al*. Adoptively transferred immune T cells eradicate established tumors despite cancer-induced immune suppression. *J Immunol* 2014;192:1286–93.
36 Dickey LL, Worne CL, Glover JL, *et al*. MicroRNA-155 enhances T cell trafficking and antiviral effector function in a model of coronavirus-induced neurologic disease. *J Neuroinflammation* 2016;13:240.

37 Overwijk WW, Theoret MR, Finkelstein SE, *et al*. Tumor regression and autoimmunity after reversal of a functionally tolerant state of self-reactive CD8+ T cells. *J Exp Med* 2003;198:569–80.
38 Antony PA, Piccirillo CA, Akpinarli A, *et al*. Cd8+ T cell immunity against a tumor/self-antigen is augmented by CD4+ T helper cells and hindered by naturally occurring T regulatory cells. *J Immunol* 2005;174:2591–601.
39 Robbins PF, Morgan RA, Feldman SA, *et al*. Tumor regression in patients with metastatic synovial cell sarcoma and melanoma using genetically engineered lymphocytes reactive with NY-ESO-1. *J Clin Oncol* 2011;29:917–24.
40 Arnaud M, Chiffelle J, Genolet R, *et al*. Sensitive identification of neoantigens and cognate tcrs in human solid tumors. *Nat Biotechnol* 2022;40:656–60.
41 Lu Y-C, Zheng Z, Lowery FJ, *et al*. Direct identification of neoantigen-specific tcrs from tumor specimens by high-throughput single-cell sequencing. *J Immunother Cancer* 2021;9:e002595.
42 Brown CE, Starr R, Aguilar B, *et al*. Stem-Like tumor-initiating cells isolated from IL13Rα2 expressing gliomas are targeted and killed by IL13-zetakine-redirected T cells. *Clin Cancer Res* 2012;18:2199–209.
43 Ohno M, Ohkuri T, Kosaka A, *et al*. Expression of miR-17-92 enhances anti-tumor activity of T-cells transduced with the anti-egfrviii chimeric antigen receptor in mice bearing human GBM xenografts. *J Immunother Cancer* 2013;1:21.
44 Johnson LA, Scholler J, Ohkuri T, *et al*. Rational development and characterization of humanized anti-EGFR variant III chimeric antigen receptor T cells for glioblastoma. *Sci Transl Med* 2015;7:275ra22.
45 Chheda ZS, Kohanbash G, Okada K, *et al*. Novel and shared neoantigen derived from histone 3 variant H3.3K27M mutation for glioma T cell therapy. *J Exp Med* 2018;215:141–57.
46 Leisegang M, Engels B, Schreiber K, *et al*. Eradication of large solid tumors by gene therapy with a T-cell receptor targeting a single cancer-specific point mutation. *Clin Cancer Res* 2016;22:2734–43.
47 Han B-S, Ji S, Woo S, *et al*. Regulation of the translation activity of antigen-specific mrna is responsible for antigen loss and tumor immune escape in a HER2-expressing tumor model. *Sci Rep* 2019;9:2855.
48 Campoli M, Ferrone S. Hla antigen changes in malignant cells: epigenetic mechanisms and biologic significance. *Oncogene* 2008;27:5869–85.
49 Woroniecka K, Chongsathidkiet P, Rhodin K, *et al*. T-Cell exhaustion signatures vary with tumor type and are severe in glioblastoma. *Clin Cancer Res* 2018;24:4175–86.
50 Wainwright DA, Balyasnikova IV, Chang AL, *et al*. Ido expression in brain tumors increases the recruitment of regulatory T cells and negatively impacts survival. *Clin Cancer Res* 2012;18:6110–21.
51 Bayik D, Zhou Y, Park C, *et al*. Myeloid-Derived suppressor cell subsets drive glioblastoma growth in a sex-specific manner. *Cancer Discov* 2020;10:1210–25.
52 Shifrut E, Carnevale J, Tobin V, *et al*. Genome-wide CRISPR screens in primary human T cells reveal key regulators of immune function. *Cell* 2018;175:1958–71.
53 Chen Z, Arai E, Khan O, *et al*. In vivo $CD8^+$ T cell CRISPR screening reveals control by fli1 in infection and cancer. *Cell* 2021;184:1262–80.
54 Stadtmauer EA, Fraietta JA, Davis MM, *et al*. CRISPR-engineered T cells in patients with refractory cancer. *Science* 2020;367:eaba7365.
55 Schaettler MO, Richters MM, Wang AZ, *et al*. Characterization of the genomic and immunologic diversity of malignant brain tumors through multisector analysis. *Cancer Discov* 2022;12:154–71.
56 Sottoriva A, Spiteri I, Piccirillo SGM, *et al*. Intratumor heterogeneity in human glioblastoma reflects cancer evolutionary dynamics. *Proc Natl Acad Sci U S A* 2013;110:4009–14.
57 Patel AP, Tirosh I, Trombetta JJ, *et al*. Single-Cell RNA-seq highlights intratumoral heterogeneity in primary glioblastoma. *Science* 2014;344:1396–401.
58 Snuderl M, Fazlollahi L, Le LP, *et al*. Mosaic amplification of multiple receptor tyrosine kinase genes in glioblastoma. *Cancer Cell* 2011;20:810–7.
59 Mahlokozera T, Vellimana AK, Li T, *et al*. Biological and therapeutic implications of multisector sequencing in newly diagnosed glioblastoma. *Neuro Oncol* 2018;20:472–83.
60 Nishikawa R, Sugiyama T, Narita Y, *et al*. Immunohistochemical analysis of the mutant epidermal growth factor, deltaegfr, in glioblastoma. *Brain Tumor Pathol* 2004;21:53–6.
61 Hegde M, Mukherjee M, Grada Z, *et al*. Tandem CAR T cells targeting HER2 and IL13Rα2 mitigate tumor antigen escape. *J Clin Invest* 2016;126:3036–52.
62 Hilf N, Kuttruff-Coqui S, Frenzel K, *et al*. Actively personalized vaccination trial for newly diagnosed glioblastoma. *Nature* 2019;565:240–5.
63 Rustenhoven J, Drieu A, Mamuladze T, *et al*. Functional characterization of the dural sinuses as a neuroimmune interface. *Cell* 2021;184:1000–16.
64 Louveau A, Smirnov I, Keyes TJ, *et al*. Structural and functional features of central nervous system lymphatic vessels. *Nature* 2015;523:337–41.
65 Chongsathidkiet P, Jackson C, Koyama S, *et al*. Sequestration of T cells in bone marrow in the setting of glioblastoma and other intracranial tumors. *Nat Med* 2018;24:1459–68.
66 Fu Y, Liu CJ, Kobayashi DK, *et al*. Gata2 regulates constitutive PD-L1 and PD-L2 expression in brain tumors. *Sci Rep* 2020;10:9027.
67 Toebes M, Coccoris M, Bins A, *et al*. Design and use of conditional MHC class I ligands. *Nat Med* 2006;12:246–51.
68 Bakker AH, Hoppes R, Linnemann C, *et al*. Conditional MHC class I ligands and peptide exchange technology for the human MHC gene products HLA-A1, -a3, -A11, and -B7. *Proc Natl Acad Sci USA* 2008;105:3825–30.
69 Sawada S, Scarborough JD, Killeen N, *et al*. A lineage-specific transcriptional silencer regulates CD4 gene expression during T lymphocyte development. *Cell* 1994;77:917–29.
70 Zhumabekov T, Corbella P, Tolaini M, *et al*. Improved version of a human CD2 minigene based vector for T cell-specific expression in transgenic mice. *Journal of Immunological Methods* 1995;185:133–40.
71 Wang Q, Malherbe L, Zhang D, *et al*. Cd4 promotes breadth in the TCR repertoire. *J Immunol* 2001;167:4311–20.
72 Nagy A, Gertsenstein M, Vintersten K, *et al*. *Manipulating the mouse embryo: A laboratory manual*. Cold Spring Harbor Laboratory Press, 2003.
73 Fleming SJ, Chaffin MD, Arduini A, *et al*. Unsupervised removal of systematic background noise from droplet-based single-cell experiments using cellbender. *Bioinformatics* [Preprint].
74 Stuart T, Butler A, Hoffman P, *et al*. Comprehensive integration of single-cell data. *Cell* 2019;177:1888–902.
75 McInnes L, Healy J, Saul N, *et al*. UMAP: uniform manifold approximation and projection. *JOSS* 2018;3:861.
76 Tirosh I, Izar B, Prakadan SM, *et al*. Dissecting the multicellular ecosystem of metastatic melanoma by single-cell RNA-seq. *Science* 2016;352:189–96.
77 Borcherding N, Bormann NL, Kraus G. ScRepertoire: an R-based toolkit for single-cell immune receptor analysis. *F1000Res* 2020;9:47.

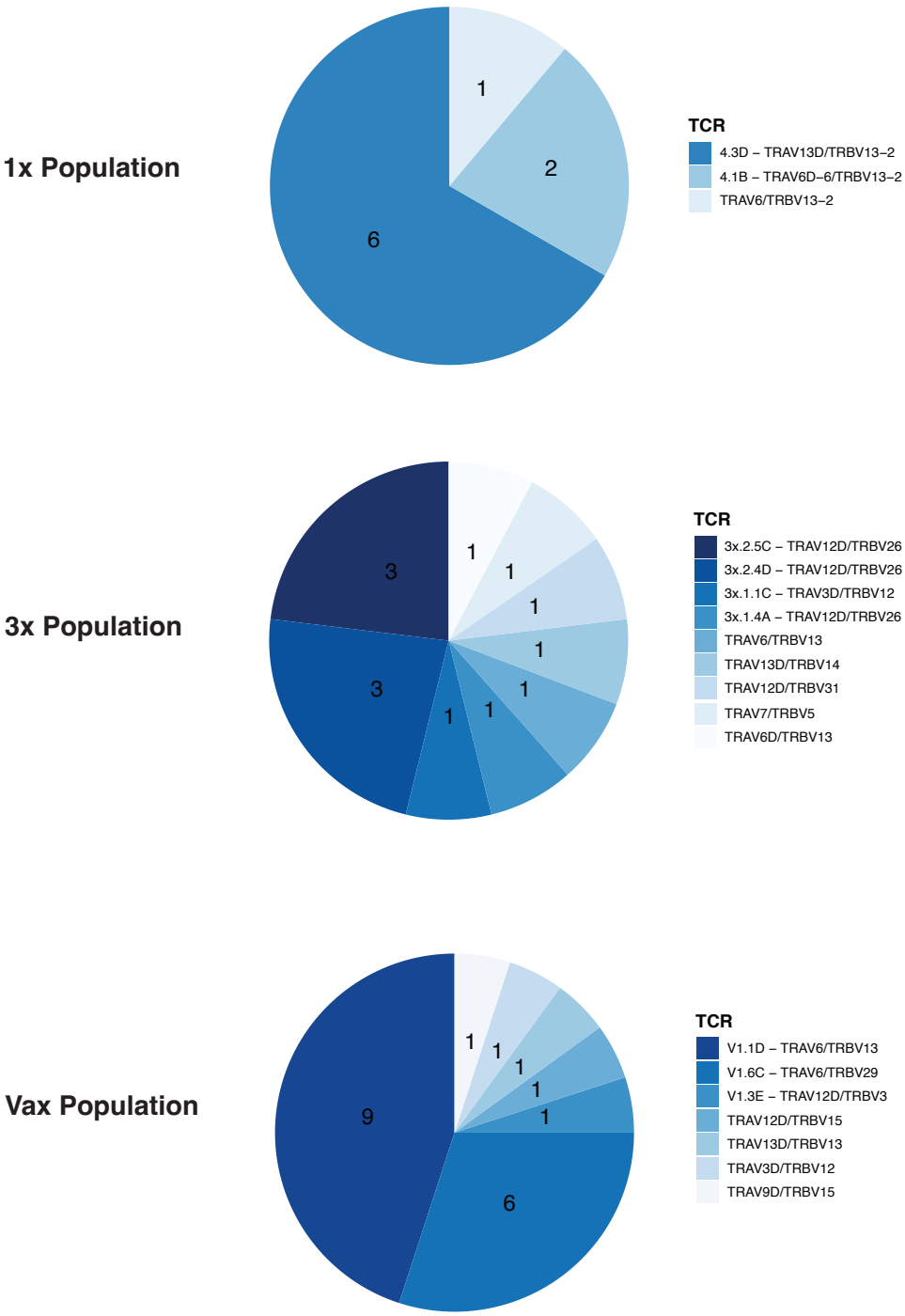

Supplemental Figure S1: Clonotype distributions of expanded populations. Pie charts depicting the frequency of each clonotype identified via single-cell PCR in either 1x stimulated splenocytes (top), 3x stimulated splenocytes (middle), or vaccine stimulated splenocytes (bottom). TCRs later screened for functional status are labeled with their specific name.

TCR	Alpha Chain	Alpha CDR3	Beta Chain	Beta CDR3
4.1B	TRAV6D/TRAJ47	CALGAEDYANKMIF	TRBV13/TRBJ2/TRBD1	CASGDWVGAETLYF
4.3D	TRAV13D/TRAJ26	CALEYAQGLTF	TRBV13/TRBJ2/TRBD2	CASGGLGDQDTQYF
V1.1D	TRAV6/TRAJ22	CVLGDSGSWQLIF	TRBV13/TRBJ2/TRBD2	CASGDAMGGAETLYF
V1.6C	TRAV6/TRAJ22	CVLAHASSGSWQLIF	TRBV29/TRBJ2/TRBD2	CASPTGGLAKTLYF
V1.3E	TRAV12D/TRAJ18	CALSDRGSALGRLHF	TRBV3/TRBJ2/TRBD1	CASSLEQGGGYNYAEQFF
3x1.1C	TRAV3D/TRAJ17	CAVGGSNSAGNKLTF	TRBV12/TRBJ1/TRBD1	CASSLEDREGSDYTF
3x1.4A	TRAV12D/TRAJ6	CALVPGGNYKPTF	TRBV26/TRBJ2/TRBD1	CASSPDSYEQYF
3x2.4D	TRAV12D/TRAJ6	CALIPGGNYKPTF	TRBV26/TRBJ2/TRBD1	CASSPDSYEQYF
3x2.5C	TRAV12D/TRAJ6	CALSEGGNYKPTF	TRBV26/TRBJ2/TRBD1	CASSPDSYEQYF

Supplemental Figure S2: Candidate neoantigen-specific TCRs. List of 9 candidate TCRs identified from single-cell PCR that were selected for further analysis with their indicated TCR characteristics.

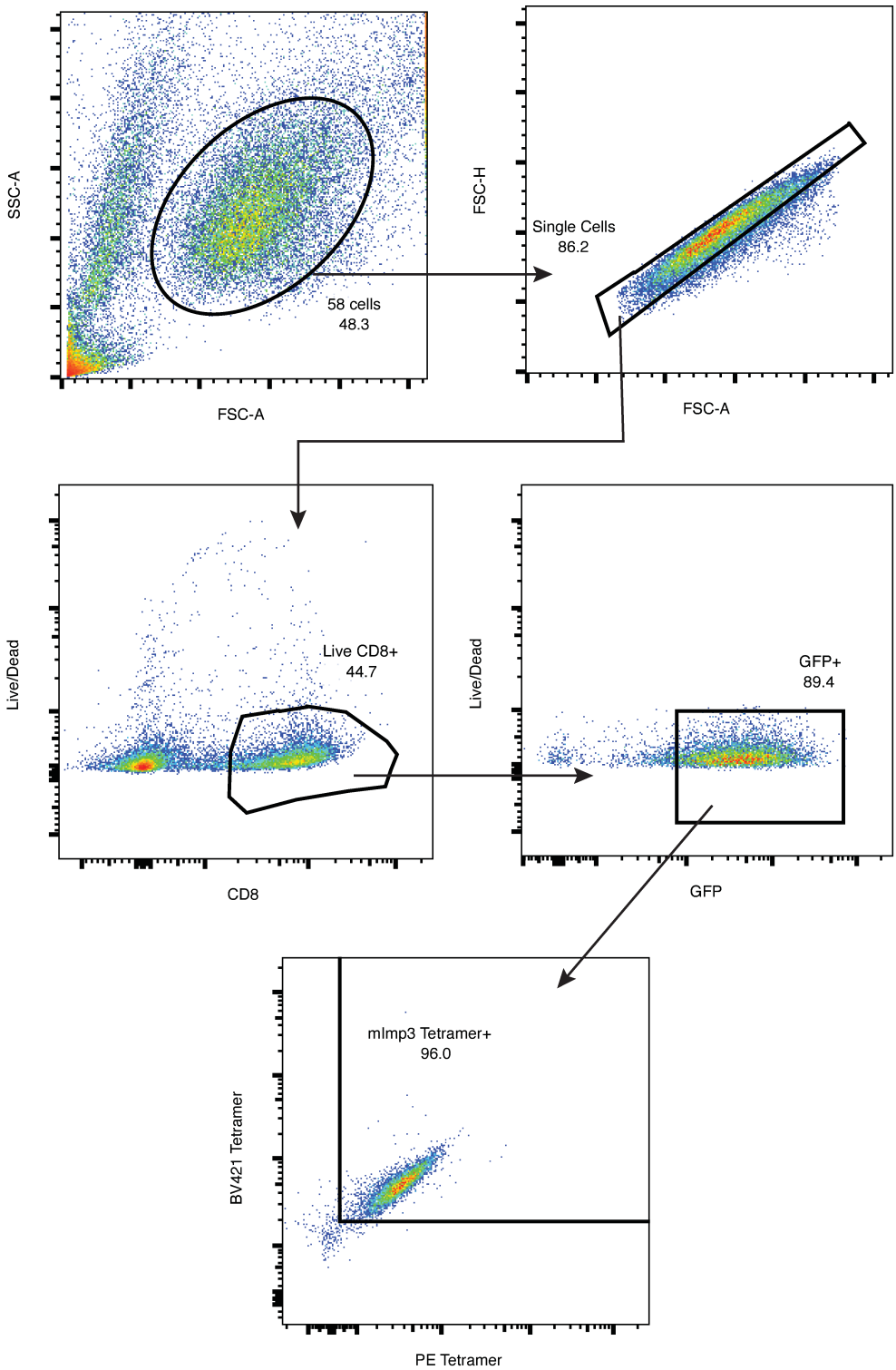

Supplemental Figure S3: Gating schema for 58 hybridoma cells. Example gating schema for 58 hybridoma cells transduced with candidate TCR (3x1.1C) and stained with cell-surface antibodies and fluorescently conjugated mImp3 tetramer.

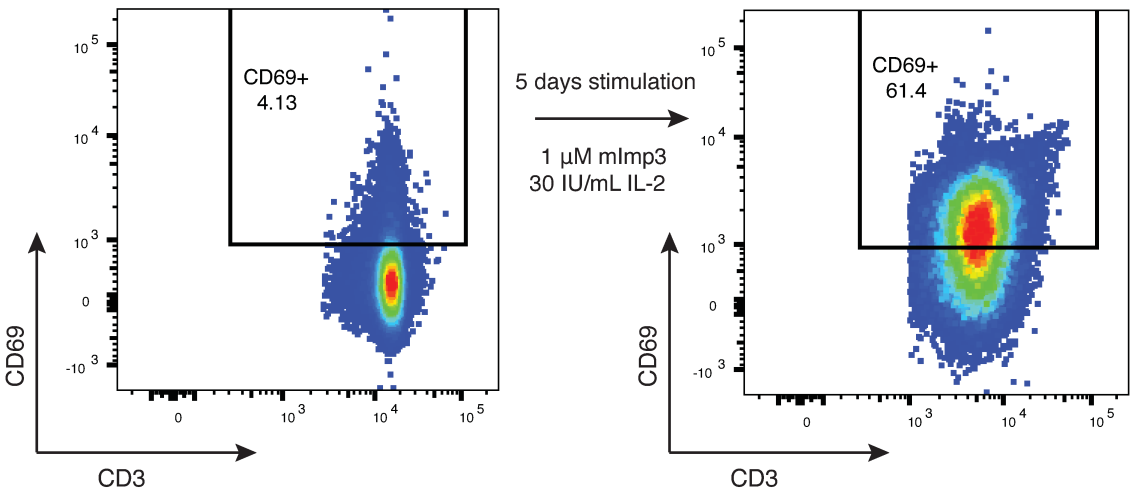

Supplemental Figure S4: MISTIC splenocyte peptide-specific activation. Representative flow cytometry plots of naive (left) or peptide-stimulated (right) CD8 T cells from the spleens of MISTIC transgenic mice after 5 days of in-vitro stimulation with mImp3 peptide and IL-2.

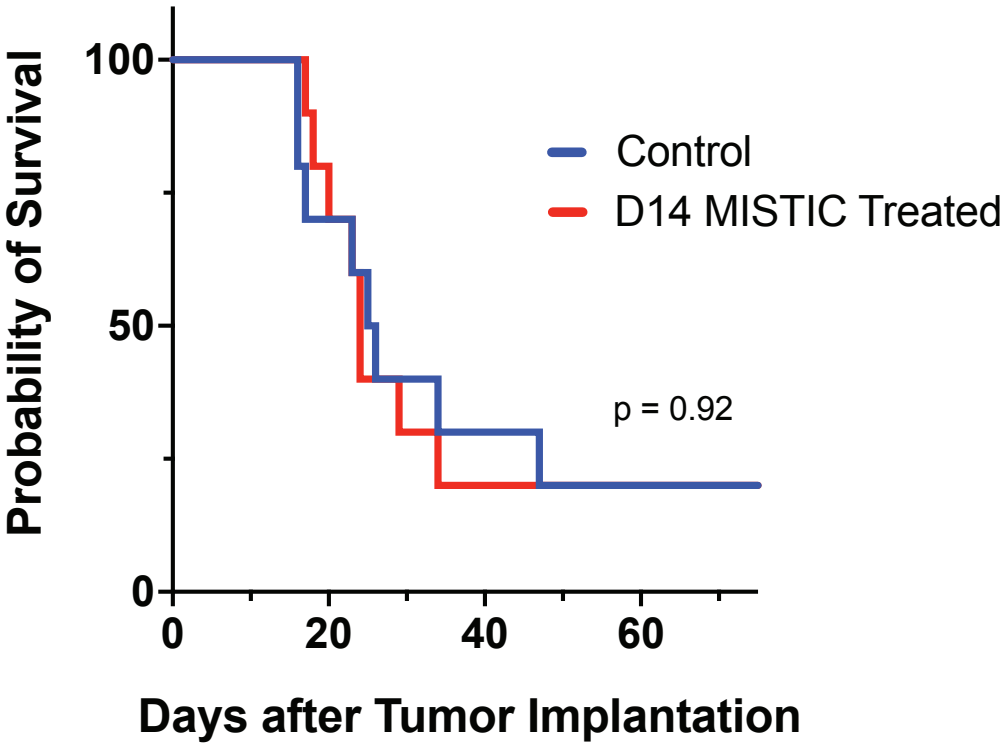

Supplemental Figure S5: Efficacy of delayed MISTIC adoptive cell therapy. Survival of GL261-bearing mice treated on day 14 with either irradiation and IL-2 (Control) or irradiation, IL-2, and MISTIC T cells (MISTIC Treated). N=10 for each group from 2 independent experiments. Significance assessed by log-rank test.

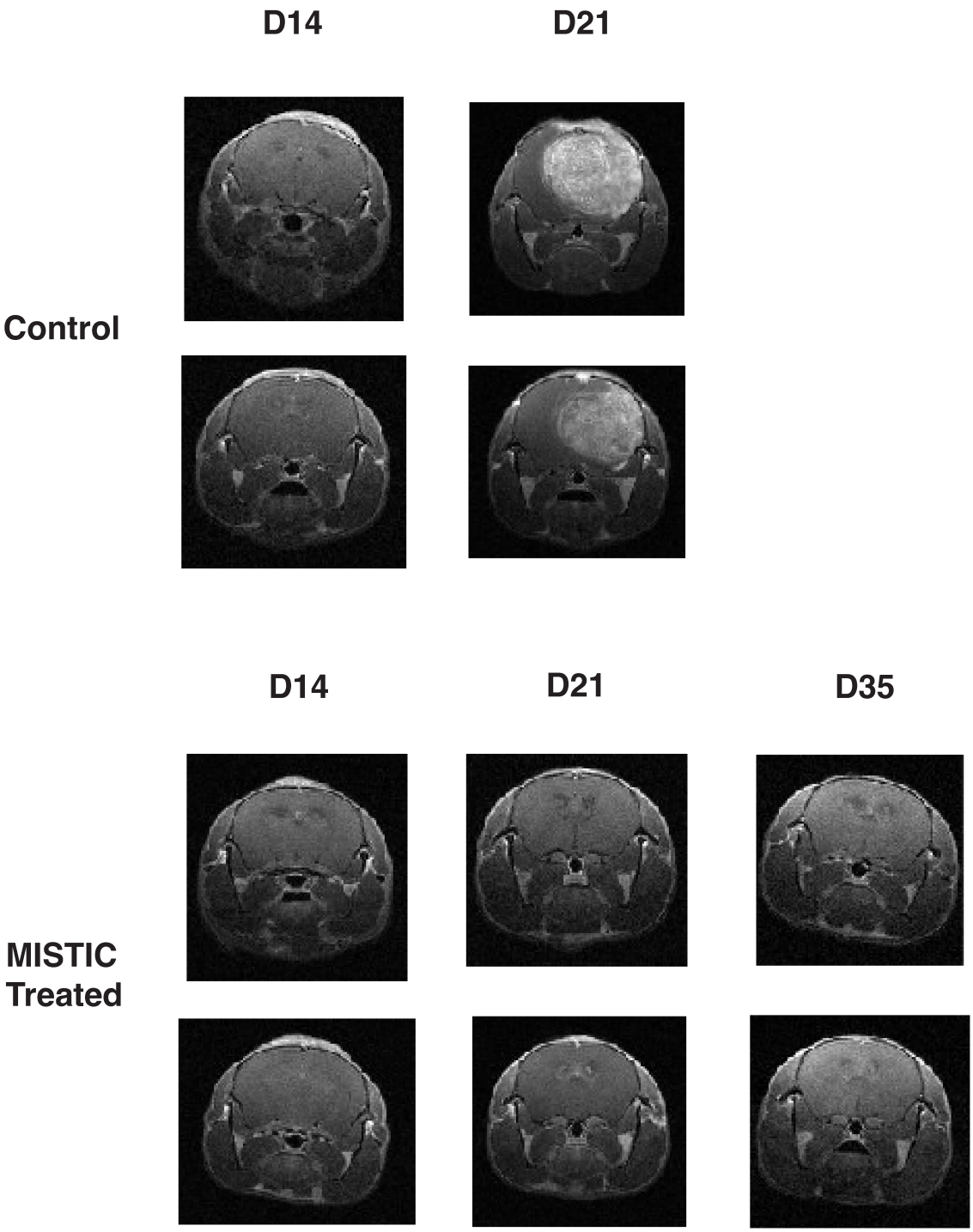

Supplemental Figure S6: Serial MRI of tumor-bearing mice. Representative T1-weighted MRI scans of either control or day 7 MISTIC treated mice 14, 21, or 35 days following tumor implantation.

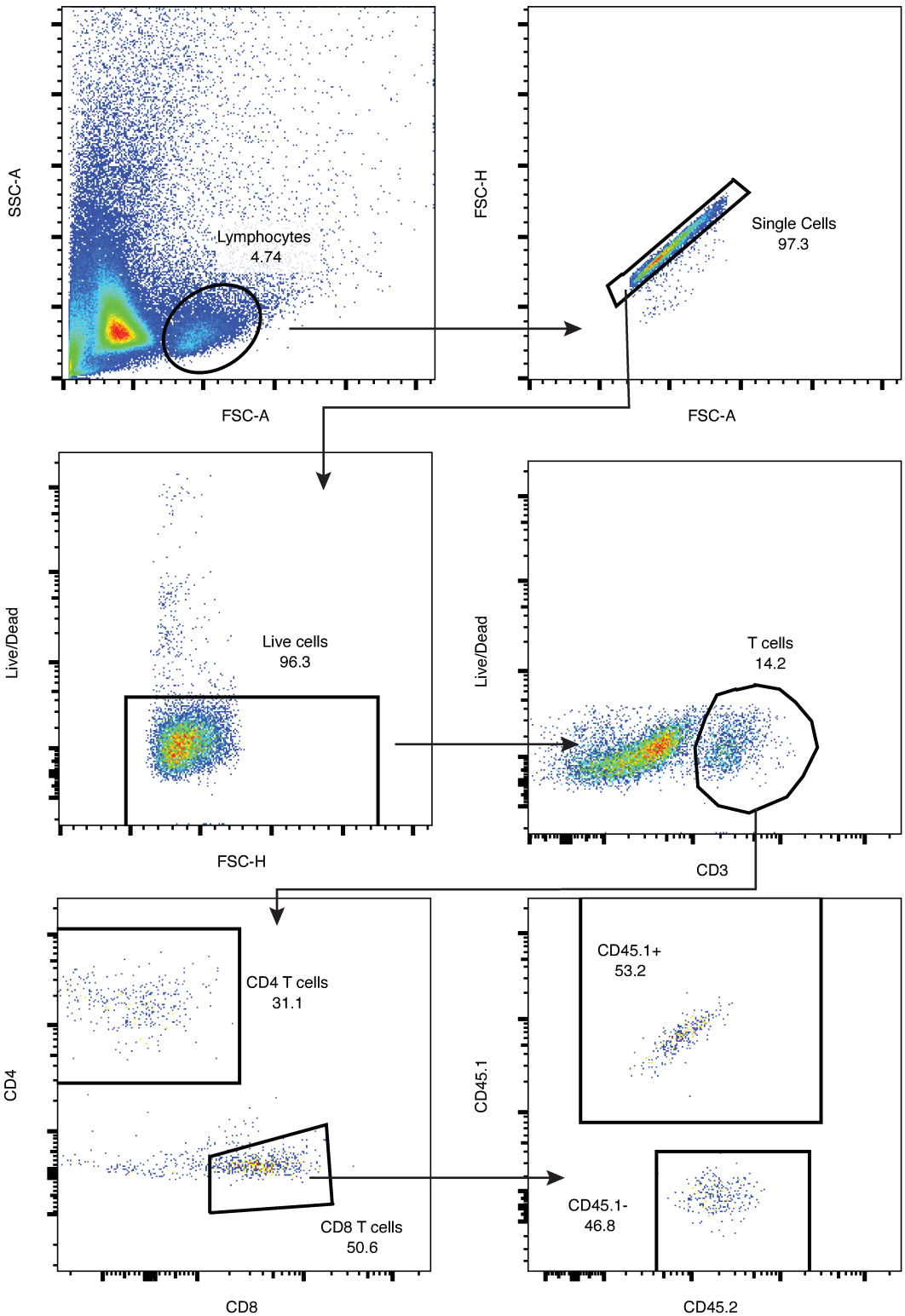

Supplemental Figure S7: Gating schema for adoptively transferred MISTIC T cells. Example gating schema for the identification of congenically labeled adoptively transferred MISTIC T cells. The provided example is from tumor tissue.

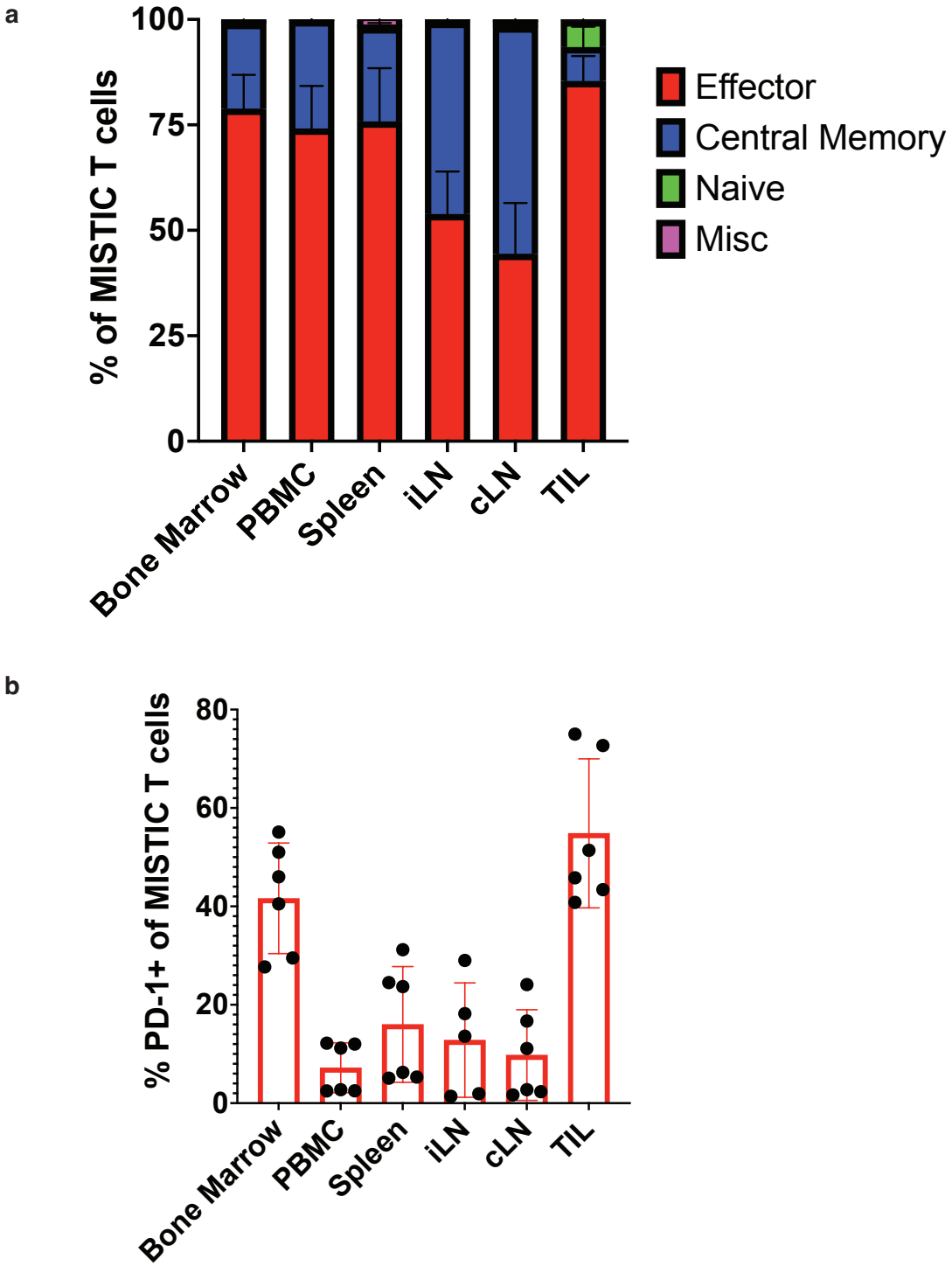

Supplemental Figure S8: Phenotypic characteristics of adoptively transferred MISTIC T cells. **a,** Stacked bar plots displaying the proportion of MISTIC T cells of a given phenotypic state in each anatomical compartment on day 10 (3 days post-transfer). Phenotypic states defined as follows: effector (CD44+ CD62L-), central memory (CD44+ CD62L+), or naive (CD44- CD62L+). N=6 from 2 independent experiments. **b,** Proportion of PD-1+ MISTIC T cells in each anatomical compartment on day 10 (3 days post-transfer). N=6 from 2 independent experiments.

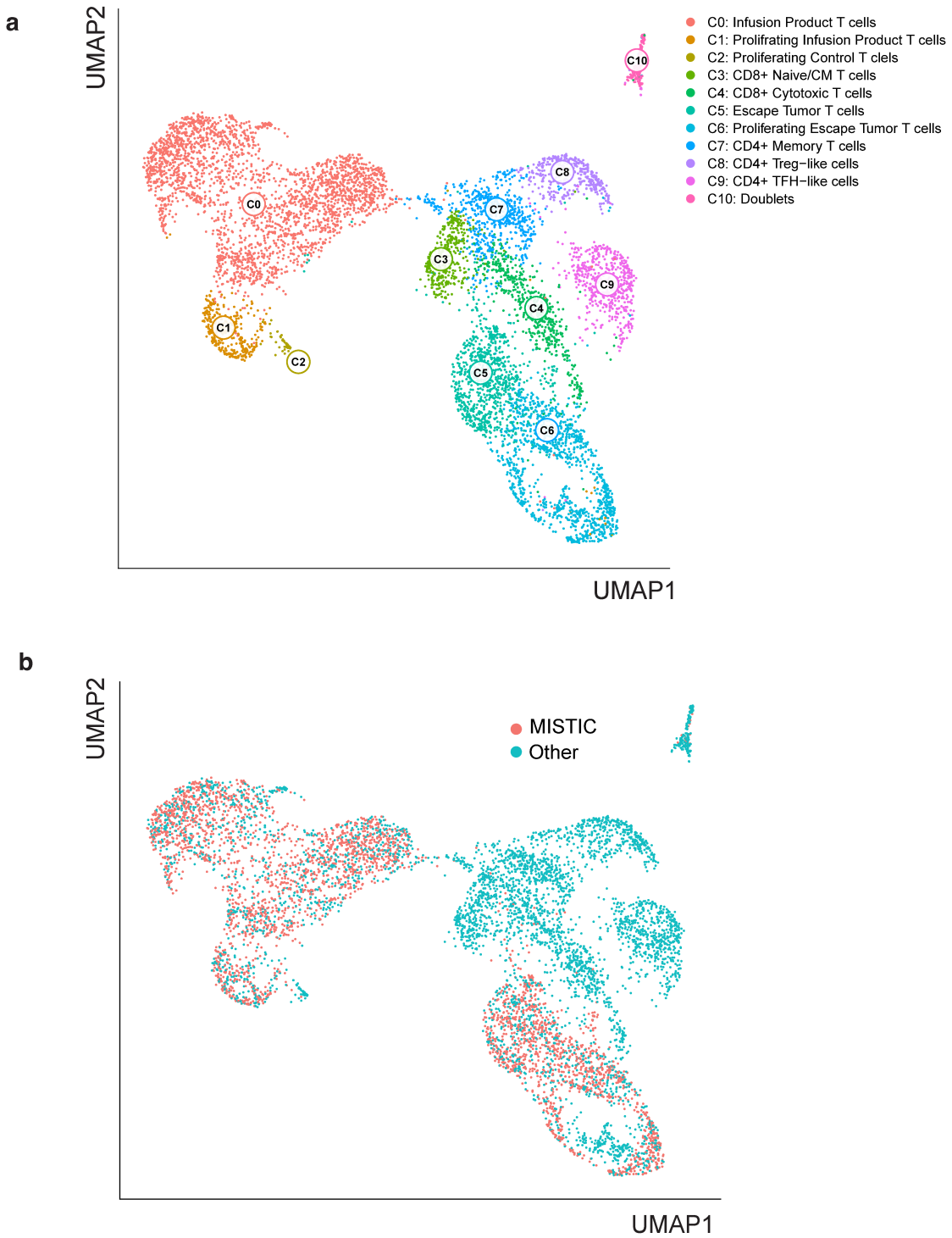

Supplemental Figure S9: Characterization of single-cell populations. a, UMAP representation dimensionality reduction of the scRNA-seq data with cell types labeled according to canonical marker genes. **b,** UMAP representation dimensionality reduction of the scRNA-seq data derived from the three populations with cells bearing the 3x1.1C TCR labeled as “MISTIC”.

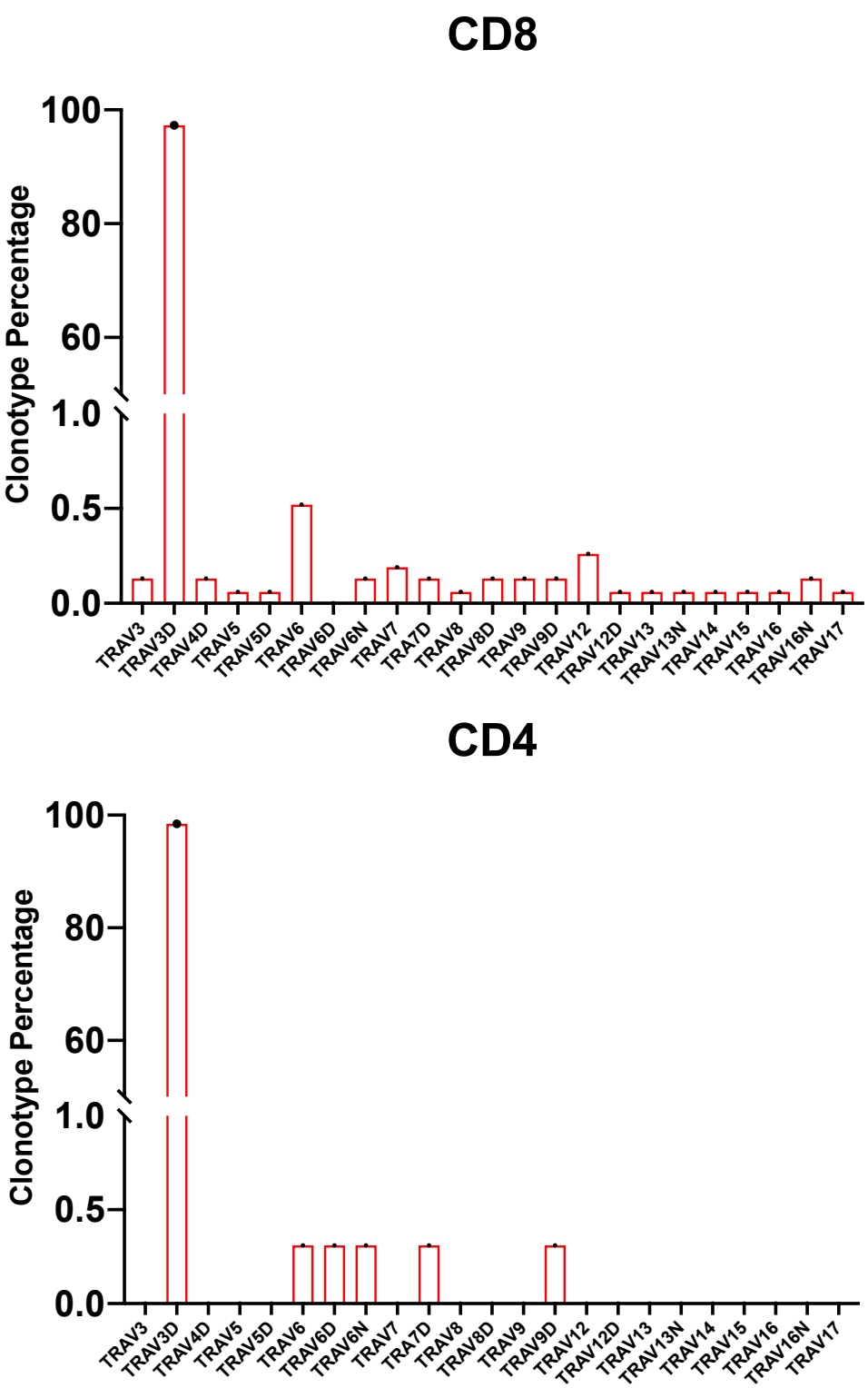

Supplemental Figure S10: Clonal architecture of MISTIC infusion product. TCR α chain usage from 1,543 CD8+ and 324 CD4+ T cells within the MISTIC infusion product as assessed via single-cell RNA-sequencing. TCR α chains not represented among either the CD8 or CD4 populations were omitted for clarity.

a

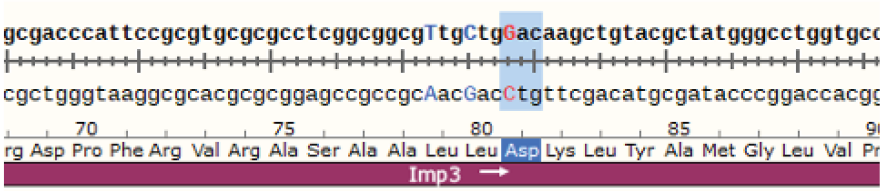

b

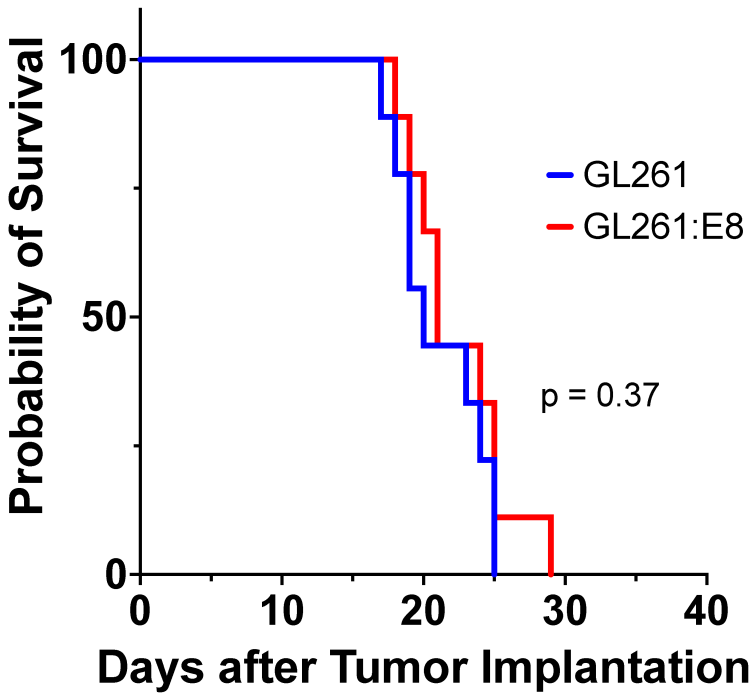

Supplemental Figure S11: Generation and characterization of GL261:E8 cell line. a, Sequencing results from the Imp3 locus in GL261:E8 confirming the N81D conversion to the wild-type Imp3 sequence. **b,** Survival of tumor-bearing mice following intracranial implantation with either GL261 or GL261:E8. N=10 mice in each group from 2 independent experiments. Significance by log-rank test.

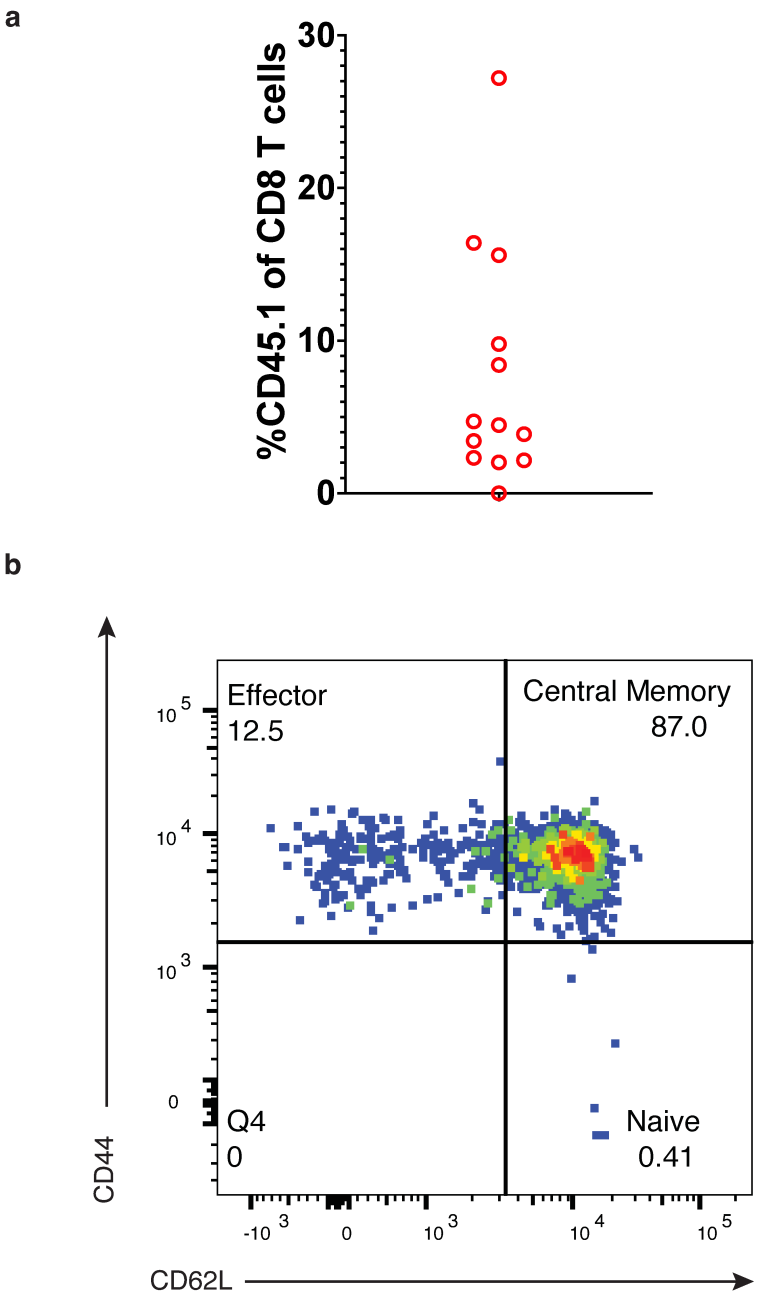

Supplemental Figure S12: Persistence of MISTIC T cells following transfer. a, Frequency of MISTIC T cells among CD8 T cells in peripheral blood of treated mice on day 50 following tumor implantation. N=13 mice from 3 separate experimental replicates. **b,** Representative flow cytometry plot displaying expression of CD44 and CD62L in MISTIC T cells in the peripheral blood of treated mice on day 50 following tumor implantation. N=13 mice from 3 separate experimental replicates.